Simulation and Implementation of an Autonomous Differential-Drive Mobile Robot for High Throughput Phenotyping

by

Jawad Iqbal

(Under the Direction of Changying Li)

Abstract

Phenotyping robots are being investigated to automate the tasks associated with high-throughput phenotyping (HTP) that can aid the development of high yield crops. The aim of this work is to develop an autonomous mobile field robot that can perform both HTP and soil sensing with the onboard LiDAR sensor and a manipulator. In the first part of the thesis, a simulation of the robot in a high-fidelity environment utilizing Robotic Operating System is presented to validate the use of an actuated LiDAR configuration that allows for simultaneous phenotyping and autonomous navigation. The use of this LiDAR configuration was shown to estimate plant height and volume with comparable accuracy to other LiDAR configurations while also navigating through crop rows with 0.2 % error. In the second part of the thesis, a differential drive robot was designed and implemented that can autonomously navigate in the field based on Global Navigation Satellite Systems. This autonomous mobile robot system validates the simulation study by implementing an actuated 2D LiDAR for both phenotyping and navigation. Additionally, a three degree of freedom articulated robotic manipulator was designed to be re-configurable and expected to perform a variety of tasks such as soil sampling and sensing. The robotic system developed in this thesis will benefit high throughput phenotyping and precision agriculture.

Index words: [Robotics, Agriculture, ROS , Simulation , High Throughput Phenotyping, LiDAR, Soil Sensing]

Simulation and Implementation of an Autonomous Differential-Drive Mobile Robot for High Throughput Phenotyping

by

Jawad Iqbal

B.S. Mechanical Engineering, University of Georgia, 2019

A [Thesis] Submitted to the Graduate Faculty of the
University of Georgia in Partial Fulfillment of the Requirements for the
Degree.

MASTER OF SCIENCE

Athens, Georgia

2020

Simulation and Implementation of an Autonomous Differential-Drive Mobile Robot for High Throughput Phenotyping

by

Jawad Iqbal

Major Professor: Changying Li

Committee: Fred Beyette
Xianqiao Wang

Electronic Version Approved:

Ron Walcott
Interim Dean of the Graduate School
The University of Georgia
August 2020

Dedication

This thesis is dedicated to Emily Nieves who encouraged me to get out of my comfort zone and pursue research. She stood by me and provided unwavering support every step of the way despite her own engagements. She sat with me and helped edit every single paragraph of my research papers (and this thesis) , assisted me in conducting outdoor robotics tests in Georgia summer heat, and most of all gave the me the motivation to keep trying despite setbacks. I'm looking forward to our next adventure and supporting her the way she supported me these past couple years.

I also dedicate this thesis to my family for giving me the opportunities that I would have never had otherwise.

Acknowledgments

I would like to acknowledge everyone who helped and mentored me in the completion of this masters thesis.

I would like to thank Dr.Li, my research mentor, who provided me the resources and mentorship needed to pursue a great thesis project.

Additionally thanks to Rui who as a more experienced peer provided support and was always being willing to answer my incessant questions.

Thanks to Hunter Halloran who also provided great and impactful contributions to my research thesis and despite just starting off is already showing the markings of a great researcher.

Thanks to Robby Ratajczak assisted with mechanical design and fabrication for my thesis project. Additionally thanks to Kevin Koffroth who made some software contributions to my thesis project.

Thanks to UGA and its undergraduate research program with which I was able to involve undergraduates with my thesis project.

Contents

[1] Published: Iqbal, J., Xu, R., Sun, S., Li, C. (2020). Simulation of an Autonomous Mobile Robot for LiDAR-Based In-Field Phenotyping and Navigation. Robotics, 9(2), 46.

List of Figures

Chapter 1

Introduction and Related Works

1.1 Motivation

Climate change, population growth, and labor shortages pose immediate threats to the sustainability of global agriculture (Campbell et al., 2018) . To ensure global food and fiber security, crop yield must increase and be made more robust. This can be achieved through breeding programs which selectively cultivate crop genotypes with favorable phenotypic traits, such as higher yield and stress tolerance (Jannink et al., 2010) . Crop phenotyping is done primarily by hand and, thus, does not allow for efficient, large-scale selective breeding (Fiorani & Schurr, 2013). In-field, high-throughput phenotyping (HTP) technologies are being developed to address this challenge, but repeatedly gathering phenotypic data on a large scale still presents a considerable bottleneck (Furbank & Tester, 2011).

To address this phenotyping bottleneck, autonomous robots equipped with advanced sensor payloads have been developed in recent years to gather phenotypic data consistently and with a high throughput. Autonomous robots are particularly useful in phenotyping applications since they reduce the human labor needed to gather large amounts of crop data. Robots can work continuously for long periods of time and at lower cost than humans, thereby allowing for a higher throughput of data collection.

In the first section of this work, a simulation of the mobile robot and LiDAR configuration is presented to validate the use of LiDAR for simulataenous navigation between crop rows and phenotyping as well as a proposed navigation algorithm. The simulated LiDAR was used to create 3D point cloud data and was tested in a high-fidelity simulation environment that mimics a cotton field with occluding effects of cotton plants and the uneven terrain of a field. This work presents a design of an autonomous agricultural robot that can navigate through crop rows and collect phenotypic data through the use of an actuated LiDAR in a "nodding" configuration (Harchowdhury et al., 2018a).

In the second section of this work, a real-world validation and design is presented of MARIA, Multi-purpose Agricultural Robot for Intelligent Agriculture. The autonomous mobile platform can perform various HTP tasks as well as navigate both indoors and outdoors using the actuated LiDAR configuration tested in simulation. An integrated robotic operating system (ROS) is also presented that handles sensor data, localization, and navigation as well as a web based GUI to allow setting waypoints.

MARIA additionally has a three degree of freedom (DoF) robotic manipulator that can perform geo-located tasks such as measure root zone temperature and humidity and collect soil samples. The onboard manipulator also has an interchangeable end effector allowing for different functionalities which is demonstrated with a soil sampling end effector design. MARIA is unique in that the platform is reconfigurable to work with other autonomous systems extrusion based design and use of off-the-shelf components and 3D prints. As such, it has the potential to be more widely available for use for HTP work as the designs are able to be replicated/modified.

1.2 Related Work

1.2.1 LiDAR-Based Phenotyping

Light detecting and ranging (LiDAR) sensors are one of the most widely used sensor systems in robotic platforms because of their ability to give accurate distance measurements without contact. LiDAR is increasingly being used in the field to generate 3D point clouds of crops for phenotypic analysis (Wang et al., 2017a) as well as low-cost crop navigation (Pabuayon et al., 2019a). A 2D LiDAR can generate point cloud data to determine important phenotypic traits of plants, such as canopy height and plant volume (Sun et al., 2017).Various methodologies have been used to calculate canopy volume from LiDAR Data. One study used a trapezoidal based algorithm where the profile of the LiDAR point cloud was used to calculate volume (Sun et al., 2018a). Another study calculated volume by voxelizing a point cloud and then extracting the volume (Jin et al., 2019). Previous studies have shown that plant height and volume are important parameters for geometric characterization and are highly correlated with final crop yield and as such are valuable measurements for selective breeding programs (Jiang et al., 2016; Zhang & Grift, 2012; Zotz et al., 2001).

A static 2D LiDAR measures distances between objects on an xy plane. These 2D scans can be combined to create a 3D point cloud by moving the 2D LiDAR and applying the transformation of the sensor's movement to the 2D scans in an inertial frame. The advantage of actuating a 2D LiDAR is that it can be used to generate a 3D point cloud at a lower cost than that of a typical 3D LiDAR sensor (Wang et al., 2017a). There exist several different 2D LiDAR configurations used to generate 3D point clouds; these are discussed in the related works section.

1.2.2 LiDAR Configurations

Most in-field applications of 2D LiDAR for high throughput phenotyping involve statically mounting the 2D LiDAR on a mobile platform and moving it directly overhead or to the side of the ground plant (Jimenez-Berni, Deery, Rozas-Larraondo, Condon, et al., 2018; Llop et al., 2016a; Sun et al., 2017; Wang et al., 2017a; White et al., 2012a). Agricultural mobile robots with side-mounted LiDAR units have been used to monitor health of crops (Bietresato et al., 2016; Vidoni et al., 2017). Two recent studies on cotton plant phenotyping using 2D LiDAR have used systems with a 2D LiDAR in an overhead configuration

in which the 2D LiDAR is perpendicular to the ground plane (French et al., 2016; Sun et al., 2017). It is important that additional 2D LiDAR configurations are evaluated to determine their efficacy in measuring plant phenotypic traits. On a mobile robot, however, the most common strategy for using 2D LiDAR is in a "pushbroom" configuration. With this configuration, the LiDAR sensor is angled obliquely to the plant, and when the mobile base moves, the LiDAR scan is "pushed" and a 3D point cloud is generated. This pushbroom configuration has been used by mobile robots to navigate between crop rows (Mueller-Sim et al., n.d.; Reiser et al., 2018). Another class of 2D LiDAR configuration for 3D point cloud generation involves actuating the LiDAR sensor while it is mounted on a mobile base; this allows the 2D LiDAR to capture additional angles for distance measurement. 2D LiDAR has also been configured with a "nodding" configuration, such that the LiDAR is on a servo and "nods" back and forth to generate a 3D point cloud (Harchowdhury et al., 2018a). In a similar but slightly different configuration, Zebeedee is spring-mounted 2D LiDAR that has been used extensively for 3D mapping commercially (Bosse et al., 2012).

1.2.3 Mobile Robots for Phenotyping

With an autonomous robot, plant traits can be measured throughout the entire growing season allowing for greater data collection and more effective plant breeding and analysis. Novel autonomous mobile platforms have been developed such as "The Robotanist," a ground-based robot able to autonomously navigate sorghum and corn crop rows as well as deploy a wide range of phenotyping sensors such as LiDAR and cameras to gather sub-canopy data Mueller-Sim et al., 2017. Another robot architecture for plant phenotyping was also presented with the "Vinobot and Vinoculer" in which a mobile ground platform (Vinobot) for individual plant inspection was paired with a mobile observation tower (Vinoculer) for overseeing an entire field Shafiekhani et al., 2017. .A low cost, 3-D printed rover, the "TerraSentia," has also been developed as an ultracompact, lightweight solution for autonomous phenotypingKayacan et al., 2018.

Large scale robots have been developed for high throughput phenotyping such as BoniRob a four wheel steering robot Ruckelshausen et al., 2009 . Thorvald where modular drive components could be reconfigured to form different drive systems Grimstad and From, 2017. An open source tracked robotic system was proposed using using off the shelf components to perform sub canopy plant phenotyping Stager et al., 2019

1.2.4 Robot Navigation

Navigation of an autonomous robot is a challenge especially in agricultural fields where the environment is semi-unstructured with uneven ground surfaces, changes daily with dust and fog affecting sensor observations, and lacks unique localization features (Mousazadeh, 2013). Efficient navigation strategies are critical to an autonomous agricultural robot in the field due to battery constraints which limit operation time. Additionally the navigation strategy must output valid velocities that are within the kinematic

constraints of the robot. GPS and range sensor-based navigation strategies are the most commonly used methods.

Navigation is another common application of 2D LiDAR as a way to allow mobile ground robots to map crop rows and therefore navigate reliably Malavazi et al., 2018a. GPS guided navigation is also typically used for field robots and allows for waypoint following in agriculture settings, but does not conduct active obstacle avoidance

A global positioning system with real time kinematic (RTK) differential correction can provide highly accurate global positioning to a centimeter level when it has an unblocked view of the satellites from the Global Navigation Satellite System (GNSS). Field robots have been developed by researchers to utilize GPS guided navigation for waypoint navigation in a world frame without any active obstacle avoidance (Bakker et al., 2010; Blackmore et al., 2004; Bonadies & Gadsden, 2019; Nagasaka et al., 2009; YANG & NOGUCHI, 2014). These waypoints are chosen to allow the rover to follow a path based on the assumption that no additional obstacles will be introduced to the rover's path. For example, "pure pursuit" is a popular path tracking algorithm that has been used extensively for autonomous navigation due to its simplicity and computational efficiency (Ollero & Heredia, 1995; Samuel et al., 2016). This navigation algorithm is a geometric method which outputs an angular/linear velocity that will move the robot in an arc to get to the desired robot position. An additional advantage of the pure pursuit algorithm is its output of a smooth path that is feasible for a differential drive robot and easily tunable with parameters such as look ahead distance. Robotanist is an agricultural robot that uses RTK GPS and "pure pursuit" as its navigation algorithm to go from point to point (Mueller-Sim et al., n.d.). PID control has also been used as a path tracking navigation system due to its robustness and simplicity in implementation (Luo et al., 2009; Normey-Rico et al., 2001). The disadvantages of GPS-based navigation strategies include that field robots may fail if the environment changes significantly or anything blocks the path of the rover (Reina et al., 2016). Additionally RTK GPS is prone to inconsistent localization due to occlusion, attenuation and multipath errors and thus it requires redundancy and continuous fail-safe checking (Rovira-Más et al., 2015). Another disadvantage for RTK GPS is that it is costly and is cost-prohibitive in multiple-robot implementations (Pedersen et al., 2006) . For inter-crop row navigation, GPS navigation is sometimes insufficient for the small heading and position corrections that are needed to successfully move between crop rows. In these cases, sensors such as cameras and range sensors (e.g., LiDAR and ultrasonic sensors) have been used extensively to perform local crop row navigation which involves determining the relative positioning (heading and distance) of the robot between crop rows (Bonadies & Gadsden, 2019). The main goal of this localization strategy is to maintain proper distance from the left and right crop rows to avoid collision (Higuti et al., 2019; Malavazi et al., 2018b; Velasquez et al., 2019). In one study, probabilistic techniques such as a Kalman Filter and Particle Filter were used alongside a 2D LiDAR for localization in-between crop rows to perform appropriate control actions (**Blok2019Navigation**). One significant hurdle using 2D LiDAR for navigation is the occlusion resulting from plant leaves and branches, which can negatively affect the characterization of the crop rows and cause navigation to fail (Higuti et al., 2019). Another important drawback of the range sensor-based navigation strategy is that it does not localize a robot in a global frame for complete autonomous control.

1.2.5 Soil Sensing and Robotics

Another important aspect of sustainable agriculture and phenotyping is characterization of soil properties such as moisture content and temperature. Phenotyping of root traits for drought resilient genotypes Passioura, 2012 is an area of particular interest due to climate change. Measuring changes in moisture content in soil gives important information on plant water-uptake rates, as well as estimating parameters such as rooting depth Bitella et al., 2014. Soil temperature is also an important quantitative measure as temperature affects root growth and architectural traits Nakamoto, 1995. Root zone temperature has an impact on stressors such as salinity He et al., 2014 and pathogen infection rates Watt et al., 2006. Soil hydraulic properties have spatial correlation ranging between 10 to 20 meters, with such variability a high number of sensing nodes in an agricultural field would be needed.

One solution to the cost of having a large amount of instrumentation is to use robots to perform these soil sensing tasks at target locations, such as a six-wheeled robot with an "e-nose" that consists of an array of six gas sensors for the detection of organic volatile compounds Pobkrut and Kerdcharoen, 2014.

Additional uses of mobile robotics have been found in the scope of soil sampling which is traditionally done manually. Bonirob, a commercial four wheel steering agriculture robot was fitted with a soil penetrometer for measurement of soil compaction Scholz et al., 2014. An additional six-wheel platform was developed to be able to take soil measurements Łukowska et al., 2019 inspired by space rovers.

1.2.6 Mobile Robotic Manipulators

In the agriculture environment, manipulators are commonly added to mobile robots to automate traditionally manual tasks. This greatly increases agricultural efficiency as mobile robots are able to work continuously and at low costs. Weeding is one common manipulator task done by mobile robots Van Der Weide et al., 2008. In one example, a manipulator mechanically uproots a weed Åstrand and Baerveldt, 2002. In other examples, actuators spray herbicide at a target location Gonzalez-de-Santos et al., 2017 such as Ladybird, a solar powered mobile robot that has a robot arm with a herbicide spray end effector Bogue, 2016. Servo-based actuators have also been developed and added to a mobile robot to perform seeding in the field Hassan et al., 2016. A mobile robot was developed with a two DoF parallel robot arm manipulator for handling paper pot seedlings Rahul et al., 2019. Robots have also been developed to mechanically evaluate crop fields using manipulators such as "Robotanist" that deployed a manipulator on a mobile robot to measure stalk strength Mueller-Sim et al., 2017 or BoniRob a four wheel steering robot to measure soil compaction Scholz et al., 2014. A prototype mobile manipulator for agriculture was proposed for general purpose use in an agricultural environment Bascetta et al., 2017.

1.2.7 Robot Simulation for Agriculture

Development of robotic platforms is time/cost intensive and complex, and, therefore, simulation is being used increasingly to test and validate robotic platforms as well as their sensors for their ability to perform agriculture sensing as well as navigation (Fountas et al., 2020; Shamshiri, Hameed, Karkee, et al., 2018).

Simulation allows for low-cost and quick robotics testing and validation, which results in a large initial focus on broad strategies. In agricultural robotic simulations, the testing environment can be recreated to match specific agricultural use cases and robotic sensor platforms, and algorithms can be tested for efficacy and efficiency (Habibie et al., n.d.; Le et al., n.d.; Malavazi et al., 2018b). Full control strategies can be tested and developed with simulated sensors completing a feedback loop. Many agricultural robot drive systems and navigation techniques have been developed and tested in simulation prior to successful implementation (Grimstad & From, 2018; Sharifi et al., 2016; Weiss & Biber, 2011) . A variety of simulation tools, such as V-REP, Gazebo, ArGOS and Webots, have been used and compared for robotics simulation in agriculture (Shamshiri, Hameed, Karkee, et al., 2018).

Chapter 2

Simulation of an Autonomous Mobile Robot for LiDAR-Based In-Field Phenotyping and Navigation [1]

2.1 Introduction

The agriculture industry is in need of substantially increasing crop yield to meet growing global demand. Selective breeding programs can accelerate crop improvement but collecting phenotyping data is time- and labor-intensive because of the size of the research fields and the frequency of the work required. Automation could be a promising tool to address this phenotyping bottleneck. This paper presents a Robotic Operating System (ROS)-based mobile field robot that simultaneously navigates through occluded crop rows and performs various phenotyping tasks, such as measuring plant volume and canopy height using a 2D LiDAR in a nodding configuration. The efficacy of the proposed 2D LiDAR configuration for phenotyping is assessed in a high-fidelity simulated agricultural environment in the Gazebo simulator with an ROS-based control framework and compared with standard LiDAR configurations used in agriculture. Using the proposed nodding LiDAR configuration, a strategy for navigation through occluded crop rows is presented. The proposed LiDAR configuration achieved an estimation error of 6.6% and 4% for plot volume and canopy height, respectively, which was comparable to the commonly used LiDAR configurations. The hybrid strategy with GPS waypoint following and LiDAR-based navigation was used to navigate the robot through an agricultural crop field successfully with an root mean squared error of 0.0778 m which was 0.2% of the total traveled distance. The presented robot simulation framework in ROS and optimized LiDAR configuration helped to expedite the development of the agricultural robots, which ultimately will aid in overcoming the phenotyping bottleneck.

[1] Published: Iqbal, J., Xu, R., Sun, S., Li, C. (2020). Simulation of an Autonomous Mobile Robot for LiDAR-Based In-Field Phenotyping and Navigation. Robotics, 9(2), 46.

This paper proposes a simulated mobile robot configuration that can collect phenotypic and crop row data and autonomously navigate between crop rows using GPS waypoints and 2D LiDAR. Using a "nodding" LiDAR configuration (Harchowdhury et al., 2018a), 3D point cloud data were generated and used for phenotyping as well as for navigation between crop rows. This actuated LiDAR configuration was tested in a high-fidelity simulation environment that simulated a cotton field with the occluding effects of cotton plants as well as the slippery, uneven terrain of a crop field that may affect LiDAR-based inferences and navigation.

2.2 Materials and Methods

2.2.1 ROS Mobile System Overview

The system modeled in this paper is an unmanned ground vehicle (UGV) called the Phenotron. The Phenotron is a 4-wheel rover that utilizes a skid steer drive system. The sensors on board the Phenotron include a Hokuyo UTM-30LX 2D LiDAR, VectorNav Inertial Measurement Unit (IMU), and a Novatel RTK Global Positioning System. A CAD model for the drive system was based on a commercially available MMP30 model (The Machine Lab, Fort Collins, CO, USA).

The Robot Operating System (ROS), an open source meta operating system, was used for the development of the Phenotron. ROS provides a standardized communication platform and system for code reuse for applications like autonomous navigation and mapping. Gazebo, an open source physics simulator, was used to simulate the cotton fields and the Phenotron. Gazebo was chosen for use in this simulation study because of its better integration with ROS and its completely open-source nature, which allows for a more extensible and widely-usable simulation. ROS was also used as the underlying communication network between the simulated sensors, the environment, and the ROS packages and open source code used for robotics development.

To import the 3D model into the Gazebo simulator, a universal robot description format (URDF) file was created where its structural and locomotion elements were defined. The SolidWorks CAD model was exported into a URDF file using the solidworks_to_URDF_exporter add-in within SolidWorks. The exporter allows the user to export a CAD assembly and its kinematic tree to a properly linked URDF file alongside its corresponding CAD files (Figure 2.1). Within the URDF, every part of the robot is defined by links and joints, with each link and joint defining various properties of the robot. The wheels are defined as links that contact the ground as the locomotion elements of the rover and have a "continuous" joint that allows for continuous rotation about one axis relative to the chassis. This continuous joint is linked from the ROS to the Gazebo simulator by defining a transmission tag that specifies a velocity joint hardware interface, which enables each wheel to send velocity commands.

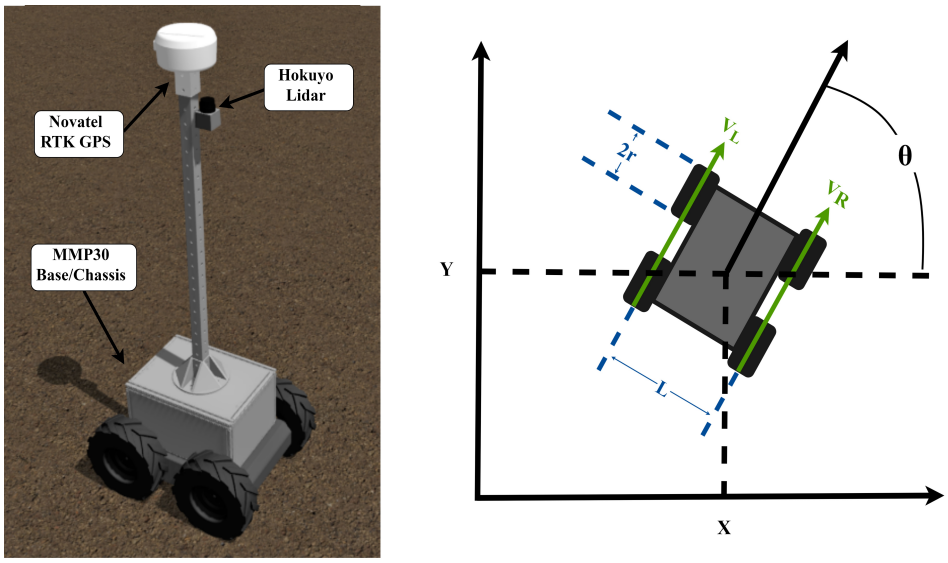

Figure 2.1: (**A**) Simulated rover Phenotron in Gazebo and (**B**) Robot kinematics V_L = average velocity of left wheels, V_R = average velocity of right wheels, θ = angle relative to X axis.

The differential drive motion of the Phenotron was controlled using the open source ROS package diff_drive_controller. The diff_drive_controller package was configured by referencing the transmission/joints defined in the URDF file and the dimensions of the rover. The diff_drive_controller accepts a geometry/twist message type that defines the linear and angular velocities along the XYZ axis. The right and left wheel velocities (Figure 2.1) required to meet the commanded goal velocity for the rover were computed and the velocity commands were sent to the rover. The diff_drive_controller package also computes the odometry of the Phenotron-simulated rover based on the velocities of the right and left wheels. Based on the odometry equations of a standard differential drive system (Equations (2.1)–(2.3)), $\dot{\theta}$ describes the angular velocity of the rover based on the linear velocities of the right and left wheels V_R, V_L in addition to the distance between the right and left wheels of the rover (L). υ is the linear velocity of the rover. With the linear and angular velocities and the heading θ of the robot, the linear velocities $\dot{x}$ and $\dot{y}$ in the world frame can be found.

$$\dot{\theta} = \frac{V_R - V_L}{L} \tag{2.1}$$

$$\upsilon = \frac{V_R + V_L}{2} \tag{2.2}$$

$$\begin{bmatrix} \dot{x} \\ \dot{y} \\ \dot{\theta} \end{bmatrix} = \begin{bmatrix} \cos\theta & 0 \\ \sin\theta & 0 \\ 0 & 1 \end{bmatrix} \begin{bmatrix} \upsilon \\ \dot{\theta} \end{bmatrix} \tag{2.3}$$

Localization sensors on the Phenotron were simulated in Gazebo through open source plugins that create a sensor interface between the simulator and the ROS. Sensor simulator Gazebo plugins for the Global Positioning System and Inertial Measurement Unit were sourced from the hector_gazebo_plugin by Team HECToR (Heterogenous Cooperating Team of Robotics) of Technische Universitat Darmstadt ("hector_gazebo_plugins - ROS Wiki", n.d.). The desired sensors/plugins are referenced in the URDF file. The sensor data were published automatically in the ROS topics list and are available for further use. For the 2D LiDAR scanner, a Hokuyo LiDAR was used with the Gazebo plugin "gazebo_ros_head_hokuyo_controller". To match real specifications of the Hokuyo LiDAR, noise was included in a parameter for the plugin such that the noise followed a Gaussian distribution with a standard deviation of 0.01 m. Thus, 99.7% of samples are within 0.03 m of the true reading, which achieves a +/- 30 mm accuracy at ranges less than 10 m (MasayasuIwase, n.d.).The simulated LiDAR has an update rate of 40 Hz. For GPS simulation, a real time kinematic (RTK) GPS was simulated including additive Gaussian noise with a standard deviation of 2 cm. With this noise factor, 70% of the time the accuracy of the GPS measurements were within 2 cm, thereby mimicking the accuracy of an RTK GPS that can achieve up to a 1 cm level positioning accuracy. The simulated GPS and IMU had an update frequency of 40 Hz. The "robot_localization" package is used to output a state estimate by using an extended Kalman filter and fusing the simulated RTK GPS with the inertial measurement unit and wheel encoder odometry. The robot localization package has an update rate of 30 Hz. For the simulated Hokuyo LiDAR, the scan frequency was 40 Hz.

2.2.2 Simulation World

A high-fidelity cotton plant model was designed within Sketchup™ and imported into Gazebo as a 3D graphic file. Once a model of a single plant was created, the plants were then rotated randomly and grouped together within Sketchup™ to create plots. The plant heights are modeled to be 1.2 m in height and 1.15 m in width and length (Figure 2.2). The plots themselves were made to be 3 m in length. The plot rows were spaced 1 m apart to mimic an experimental cotton field. The size and spacing of the plots were based on a study where multiple cotton plant cultivars were analyzed in terms of growth (Sun et al., 2018a). There were five plants within each plot with a 0.6-m distance from each other to have around 50% overlap to simulate plant occlusion and density.

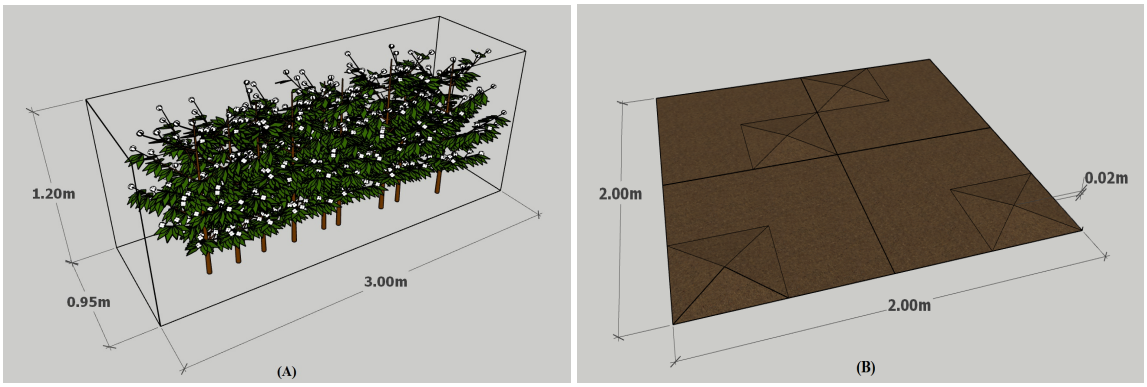

Figure 2.2: (**A**) Dimensions of the cotton plot and (**B**) a section of ground floor.

The ground was constructed in Sketchup™ using the sandbox tool. Bumps were simulated by creating pyramid-shaped protrusions in the plane's mesh with the height of the bumps being 2 cm. This height was decided based on a reference (Kragh et al., n.d.) in which agricultural terrain was classified. Four 1 × 1 m squares with arbitrarily chosen "bumps" were put together randomly to make a 2 × 2 m (Figure 2.2). In this configuration, there was a 100% chance that the rover would encounter some type of bump disruption per two meters of travel. Then these 2× 2 squares were multiplied to create a 60 m by 60 m field. A testing field of 4 rows was created in which each row consisted of 3 plots and in which each row was spaced 1 m from each other (Figure 2.3).

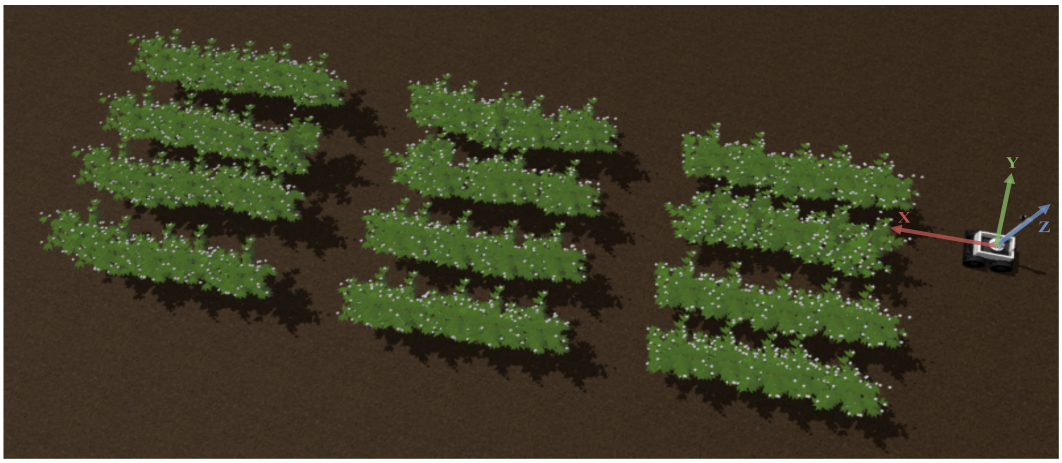

Figure 2.3: Test field for LiDAR-based phenotyping.

2.2.3 Experiment/Analysis Phenotypic Analysis

LiDAR Configurations

Multiple LiDAR configurations that have been used in HTP were configured and tested on a simulated cotton field. Their ability to correctly identify the height and volume of the plants using a 2D LiDAR was

evaluated. The proposed actuated LiDAR configuration, also known as "nodding," was tested against 3 common static LiDAR configurations used in agricultural robots for phenotyping: Tilted, Side and Overhead. The Tilted configuration was angled 45 degrees down from horizontal, aimed obliquely at crops at a height of 1.5 m (Figure 2.4A) . The Side configuration was angled perpendicular to the ground, facing directly to the side of the crops at a height of 0.75 m (Figure 2.4B) . And finally, the Overhead configuration was pointed towards the ground and facing the crops directly overhead (Figure 2.4C). The proposed LiDAR configuration actuates the 2D LiDAR in a nodding motion, similar to the Tilted configuration. However, the LiDAR angle is relative to horizontal changes over time (Figure 2.4D). This strategy is proposed to address leaf occlusion because some features are lost as the LiDAR needs a clear path to detect the profile of the plant canopy accurately, and, as such, multiple angles of detection would assist in this characterization (Pabuayon et al., 2019a). For the nodding configuration, the LiDAR is rotated while the mobile base is static and the angled LiDAR scans from 0 radians (parallel to the ground) to 0.4 radians (22.9 degrees) towards the ground. The LiDAR is actuated at a step increment of 0.005 radians (0.286 degree) at 10 Hz which results in a rotational velocity of 0.05 radians a second (2.86 degrees) and a complete nod cycle time of 8 s.

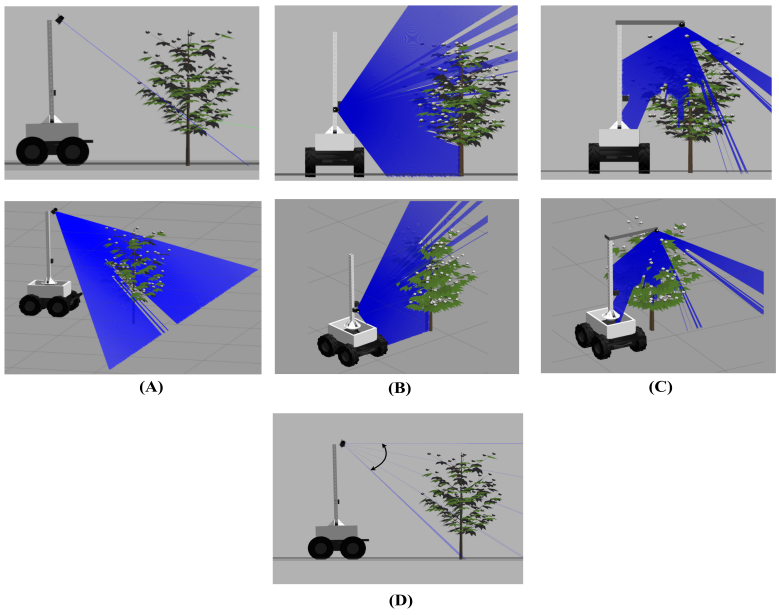

Figure 2.4: LiDAR configurations: (**A**) Tilted , (**B**) Side , (**C**) Overhead, and (**D**) Nodding.

Since only a 2D LiDAR was used, each scan of the LiDAR needed to be stitched together to generate a 3D point cloud for analysis. The laser assembler ROS package was used to initiate a server service that could be called upon to begin assembling scans together at specific time intervals. The frame in which these laser scans were assembled was set with the laser assemble ROS package and in the global "map" frame (Figure 2.5) . This transform frame is generated by the "robot_localization" package. The "laser_assembler" service call responds with a point cloud that is then published to an ROS topic. This assembled laser point cloud

is then downloaded as a PCD file using the *pcl_ros* package, which listens to a topic and then saves it to a directory.

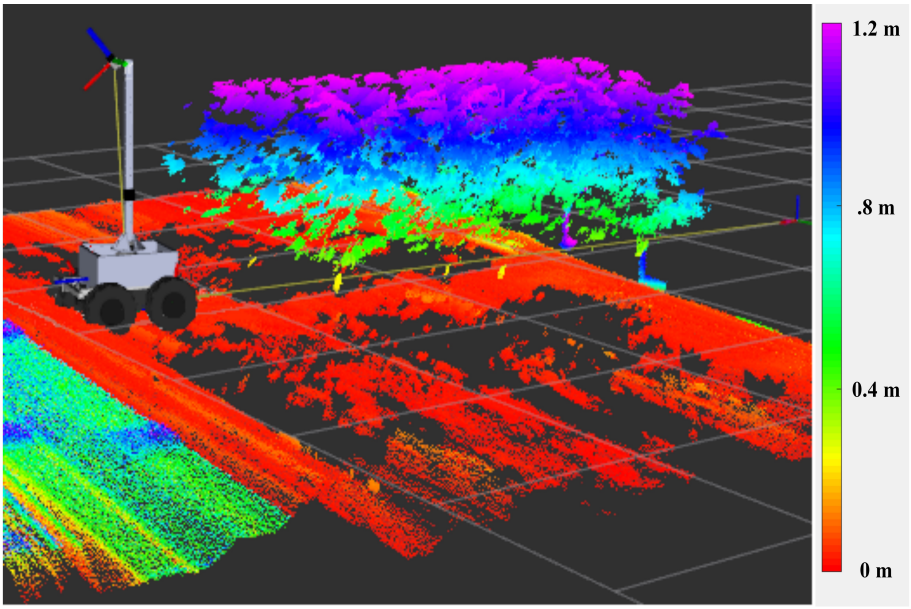

Figure 2.5: Assembled LiDAR on uneven terrain data visualized within RVIZ using the Tilted configuration.

The ability of the LiDAR configurations to obtain the two main phenotypic traits of cotton plants, height and volume, was tested (Figure 2.6). For each of the 4 LiDAR configurations, the simulated autonomous robot was given a velocity command to go forward and continuously collect LiDAR data for a single row containing 3 plots (Figure 2.5). Each configuration collected point cloud data (PCD) from a single side of the plot for phenotyping estimation. After data collection, the resulting PCD was post processed in MATLAB. A region of interest (ROI) was manually selected for each plot for processing, then the ground floor was determined by using the random sampling consensus algorithm (RANSAC). Once determined, the ground floor was also removed, although the height of the ground plane was recorded as the baseline for height prediction.

To obtain plant height, the LiDAR data were projected on the XZ plane such that height measurements were calculated along the axis that the mobile rover base traveled. Then, peaks were filtered from the height data such that each peak was higher than the peaks around it at a certain distance threshold (Jiang et al., 2016).

To obtain the ground truth for plant volume, the CAD model for the cotton plot was voxelized with cubic centimeter voxels which are cubic volumetric shapes representing regularly sampled spaces that are non-homogeneously filled. The voxelization of a CAD model allows for the computation of volume taken up by the CAD model with a predetermined sized cubic shape. The voxelized plant model was put into a CAD program called Blender where the 3D print tool was used to determine the volume of a single voxelized cotton plot. The volume of a single plot was experimentally determined from the point

cloud data using the MATLAB boundary function with its default shrink factor of 0.5. Shrink factor is a scalar value ranging from 0 to 1 where 0 results in the convex hull of the points while 1 corresponds to the tightest single-region boundary around the points. As such when the shrink factor was 1, due to making the tightest boundary around the point cloud, the volume estimate is much lower than when the shrink factor was 0 where only the outer most points are used for the generated hull. The default value for shrink factor of 0.5 was kept as it was a neutral parameter for volume estimation.

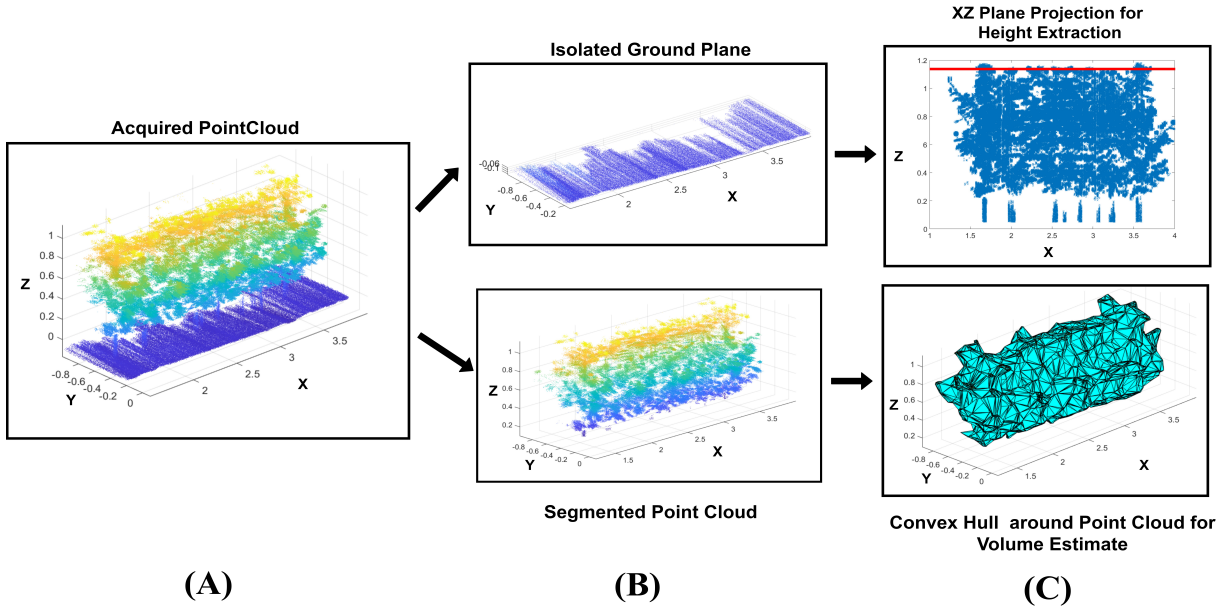

Figure 2.6: LiDAR phenotyping pipeline to extract phenotypic traits. (**A**) A point cloud generated from the Nodding LiDAR configuration, (**B**) The PCD is split into the ground plane and segmented point cloud of a single plot , (**C**) The isolated ground plane is used as a datum for calculating height of segmented point cloud and convex hull is used just on the segmented point cloud for volume estimation.

2.2.4 Experiment/Analysis Nodding LiDAR Configuration for Navigation Through Cotton Crops

As the rover moved through the crop row, the 2D LiDAR was actuated in a certain "nod" window. In this nod window, 2D laser scans were stitched together to generate a 3D point cloud at a certain look ahead distance. Since the rover is in the middle of the two rows, the field of view of the 2D LiDAR is large enough to capture both the left and right crop row simultaneously at each nod. While the LiDAR unit is actuating, the laser assembler node is continuously listening to the LiDAR topic and the transform of the LiDAR unit to assemble the individual scans and generate a point cloud every 8 s which is the time needed to complete a single nod. The Hokuyo LiDAR is continuously being actuated to make sure that the crop rows are being characterized even while moving. The LiDAR scans are still being transformed and assembled relative to the movement of the rover itself as it is moving by using the state estimate and

transform provided by the "robot_localization" package. The output of the "robot_localization" state estimation is at the same frequency as the simulated Hokuyo LiDAR, as such the pose of the robot is accurately considered even while moving. At the end of each “nod” action, the generated point cloud was sent to a Python service node in the sensor_msgs/PointCloud2 message format. This Python service, which is detailed later, returned the angles of the left and right crop row as well as their distance away from the rover. Based on this service response, the navigation module performs a control action which would include angular and linear velocity for 0.25 s. Then the rover waits for the next control update as the nodding LiDAR gets actuated and the point cloud data gets processed. The main goal of the LiDAR based navigation strategy was to stay parallel and equidistant with the left and right crop rows. Each point cloud generated for every iteration of the looped navigation control were combined based on the distance traveled by the rover as calculated by the "robot_localization" package.

LiDAR Processing Strategy

Using the same laser assembler package discussed above, the nodding LiDAR scans were assembled within a specific tilt window. The tilt window was defined as the angle range at which the nodding actuation occurs and the corresponding 2D laser scans assembled into the point cloud. A row_characterization service server was created that accepts a point cloud from the assembled point cloud topic. The row_characterization server utilizes the open 3D point cloud library, a library for point cloud data processing. The point cloud data were downsampled and voxelized and then split into the left and right rows (Figure 2.7). Each of these rows were then filtered using a radius outlier filter and then a RANSAC algorithm was used to fit a line through the left and right rows. The row_characterization server returned the average angle of the left and right crop rows as well as the distance of left and right rows from the robot itself.

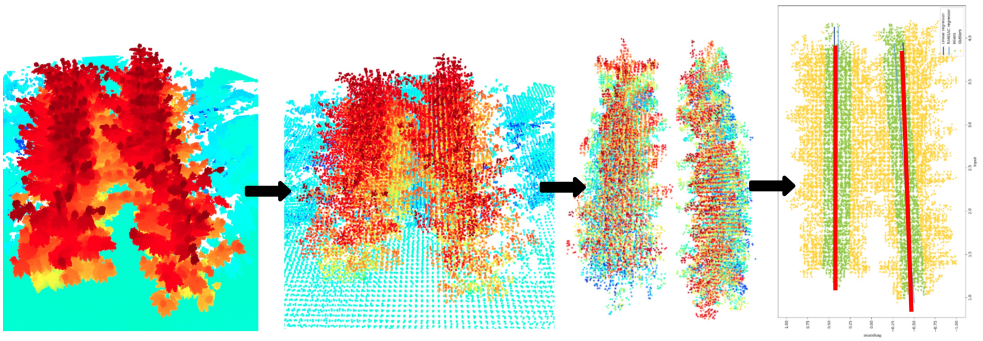

Figure 2.7: LiDAR crop row characterization strategy: (**A**) generated point cloud from actuated LiDAR, (**B**) downsampled and voxelized point cloud, (**C**) left and right split crop rows with radius outlier filter, (**D**) left and right crop row characterization using RANSAC.

2.2.5 ROS Node Structure

A complete ROS topic and node structure was developed to mimic the topic and information structure of the real rover (Figure 2.8). The data from the inertial measurement unit, wheel odometry, and GPS topics were combined using an extended Kalman filter using the robot localization package to get an accurate pose estimate. The robot localization package also handled creating the various transforms needed to convert GPS waypoints into goals in the rover's frame. The GPS topic was converted to UTM coordinates by the *gps_common* package for Euclidean-based navigation. A navigation module was developed to handle all control actions of the rover and the implementation of the algorithm described above. An ROS service was created that takes a point cloud input in the sensor_msgs/PointCloud2 ROS message format. The service call processed the point cloud and characterized the crop row point cloud to give the angles of the left and right crop rows and the distance between them. The navigation module then processes the crop row information and performs the appropriate control action. ROS-control and Gazebo are simulation-based processes that implement commands to actuators and simulate all sensor and physical interactions with the rover.

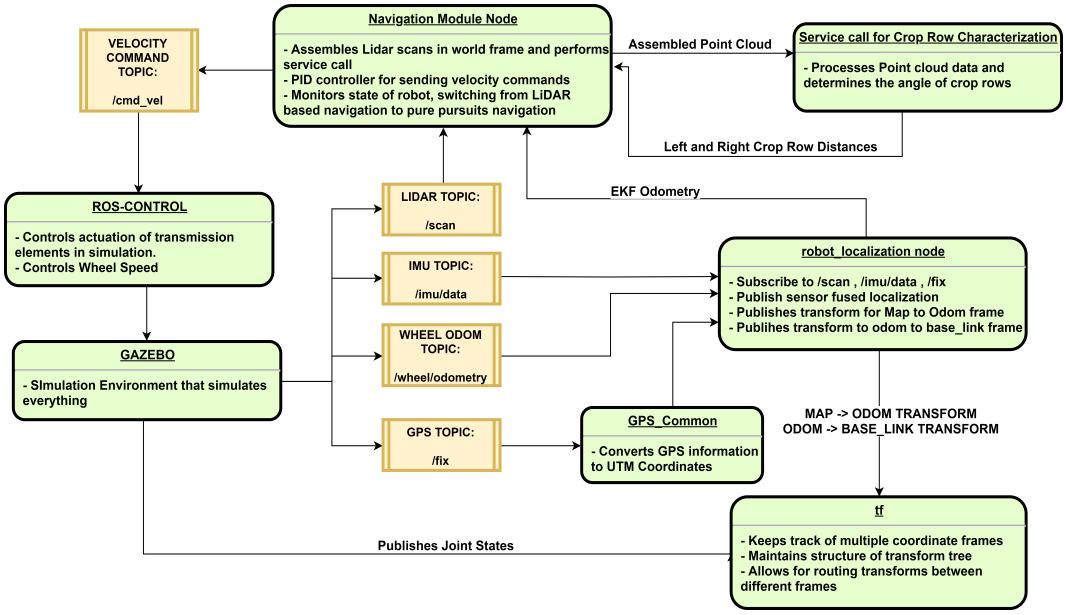

Figure 2.8: ROS node diagram.

Control Loop for Crop Row Navigation

A feedback system with two error signals was created to correct the rover to ensure it is traveling safely between the crop rows. One error signal includes an angle of the rover relative to the left and right crop rows. Ideally, the robot should be completely parallel to the left and right rows. If the crop rows are angled from the rover's perspective, the angles of the left and right crop rows are averaged and then this is output as an error for row heading. The average of the left and right rows was used as the error signal. The

second error signal was the difference in distance between the robot and the right and left rows. Ideally, the difference between the two rows would be zero, which would mean that the right and left rows are equidistant from the robot, which is the desired position of the robot. If the position was closer to the right row than the left row, this would be output as an error. For the heading error and the distance error there were threshold values for registering errors to make sure that the control action was not enacted for trivial error values in heading and distance. The error values for heading and distance are multiplied by corresponding weights C1 and C2 to control the amount of impact each error signal has on the control action (Figure 2.9). Then both error signals are summed and input into the PID controller. The PID controller was tuned through trail and error to output the appropriate angular velocity for 0.25 s to correct the heading and the centering of the rover relative to the crop rows. For each control step, there was always a linear velocity in the x-axis frame to ensure the robot keeps on moving forward. The control loop iterated based on the subsequent error signals generated by the actuated LiDAR until the stop condition is met as described by the complete navigation algorithm detailed below.

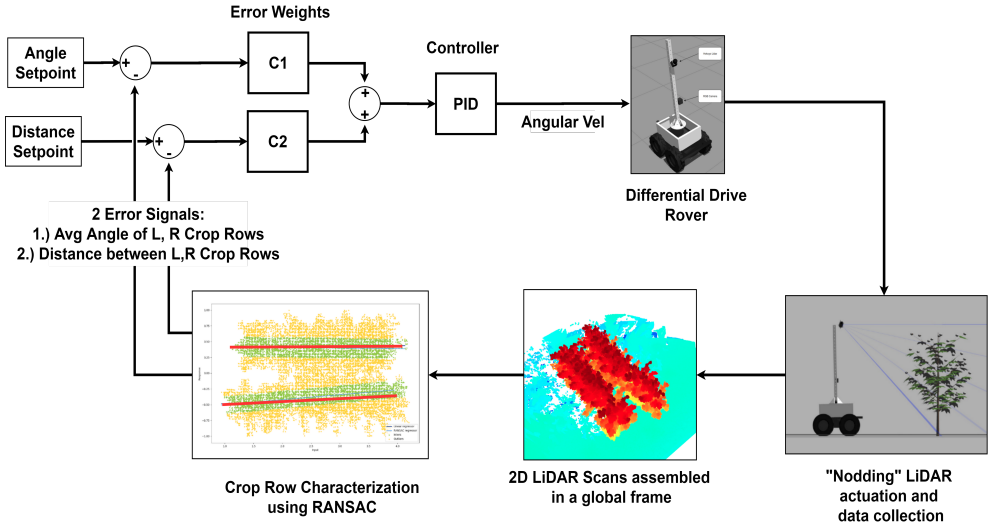

Figure 2.9: Control loop for crop row navigation.

Complete Navigation Algorithm

A simple navigation algorithm was implemented for use with the LiDAR based navigation strategy (Algorithm 1). The LiDAR based navigation strategy was designed to be able to move within crop rows despite occlusion and misaligned crop rows without any global positioning. However, for use in a crop field with multiple rows, additional intelligence is needed. An algorithm is proposed that switches between the LiDAR based navigation, which is robust in navigation between crop rows, and a GPS-based navigation strategy, which ensures that the robot is going to the correct user-defined crop row. The GPS guided navigation algorithm used is called the Pure Pursuit, which finds the linear and angular velocity needed to go to a specific point in space (Mueller-Sim et al., n.d.).

Algorithm 1: Complete Navigation Algorithm

Result: Complete navigation of crop rows
d_{cr} = distance between crop rows;
d_{wp} = distance to next waypoint;
while *Not at last GPS waypoint* **do**
    if $d_{wp} > d_{cr}$ **then**
        Perform LiDAR based navigation;
        Update d_{wp};
    end
    if $d_{wp} < d_{cr}$ **then**
        Perform Pure Pursuit navigation to next waypoint;
        Once waypoint is reached, next waypoint is updated;
    end
end

The proposed algorithm creates a robust navigation strategy that is extensible and re-configurable for different navigation plans for the rover. The main parameter in this algorithm is the distance between crop rows (d_{cr}) (Figure 2.10). Initially, the rover starts using the LiDAR-based navigation strategy when it goes straight while facing the next GPS waypoint. However, when the rover is within (d_{cr}) distance of a GPS waypoint, it switches to the Pure Pursuit algorithm. The Pure Pursuit algorithm guides the rover to the waypoint (A GPS coordinate as well as heading), which faces the next waypoint on the list of waypoints given by the user (these are points between one crop row plot and the next to define the path the rover will take). When the rover gets to the waypoint at a sufficient tolerance and faces the next waypoint, the navigation algorithm now switches back to the LiDAR-based navigation strategy. The rover goes straight while performing an appropriate control action to stay centered between crop rows until it gets within d_{cr} of the next waypoint and the algorithm repeats until the last waypoint. In the case where it reaches the end of the crop row and must go to the next crop row, it checks the (d_{cr}) parameter and automatically switches to Pure Pursuit to get into position to implement the nodding LiDAR-based navigation. This process will continue until the last waypoint is reached. With the switching dual strategy, fewer waypoints are needed to be given to the rover, and by being given only the waypoints at the end of each row, the LiDAR-based navigation strategy can maintain distance between crop rows successfully.

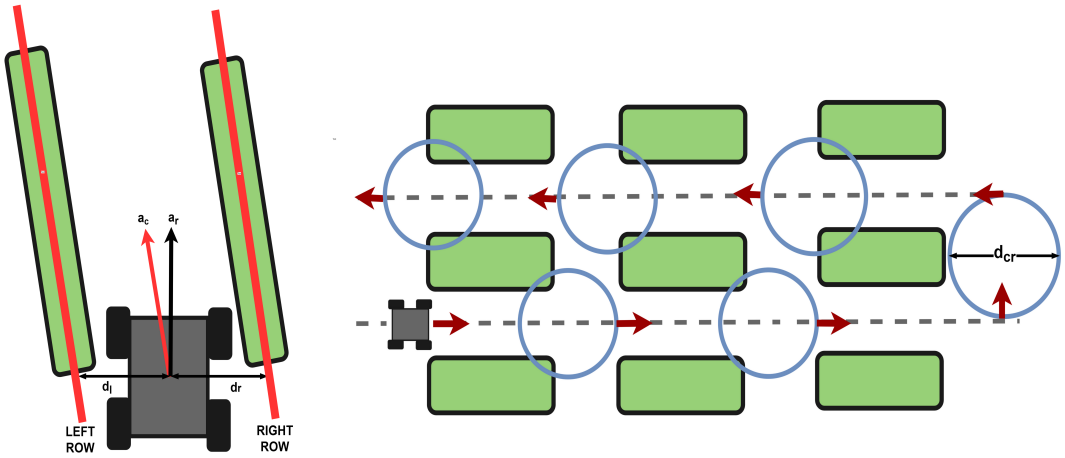

Figure 2.10: (**A**) Robot heading definition, d_r and d_l : Distance from left and right crop row respectively, a_c and a_r : angle of the crop rows and angle of the robot respectively; (**B**) navigation strategy, d_{c_r} = distance between crop rows.

The navigation strategy was tested in a simulated crop field under two scenarios. In the first scenario, the crop rows were parallel with each other and waypoints were provided for each plot totalling 12 waypoints. In the second and more challenging scenario, the crop rows were not parallel, which allowed for the testing of the robustness of the navigation strategy to make corrections for non-parallel crop rows. Additionally, the test waypoints were given only at the end of the crop rows totalling 6 waypoints, so the LiDAR-based navigation strategy had to navigate through the entire crop row by itself. The ideal path was determined as being equidistant and parallel to the crop rows.

2.3 Results and Discussion

2.3.1 Phenotyping and Navigation Results

The nodding, tilt and side configurations had comparable volume results with an average percent error of 6%. Of the 3 configurations, the nodding configuration had the highest volume error of 6.6% $\pm$ 4.8%. The tilt and side LiDAR configurations had average errors of 5.7% $\pm$ 3.4% and 6.6% $\pm$ 2.8%, respectively (Figure 2.11). The tilt and nodding configurations had the most similar results, however the nodding configuration performed slightly worse due to the LiDAR actuating while moving over the uneven ground. The side configuration performed slightly better than the tilt and nodding configurations due to having the best side profile of the plot as well as being the best suited for the convex hull method of volume estimation. The side configuration was able to get the ends of the plots which due to getting a hull wrapped around it, compensated for not having a view of the width of the plot. The overhead configuration had the highest average percent error for volume at 15.2% $\pm$ 5.7%. While all the volume estimations were underestimates

compared to the ground truth, the overhead volume estimate was much lower. This underestimation from the overhead configuration was due to the LiDAR only being able to view the canopy of the plot and missing the side profile for volume estimation.

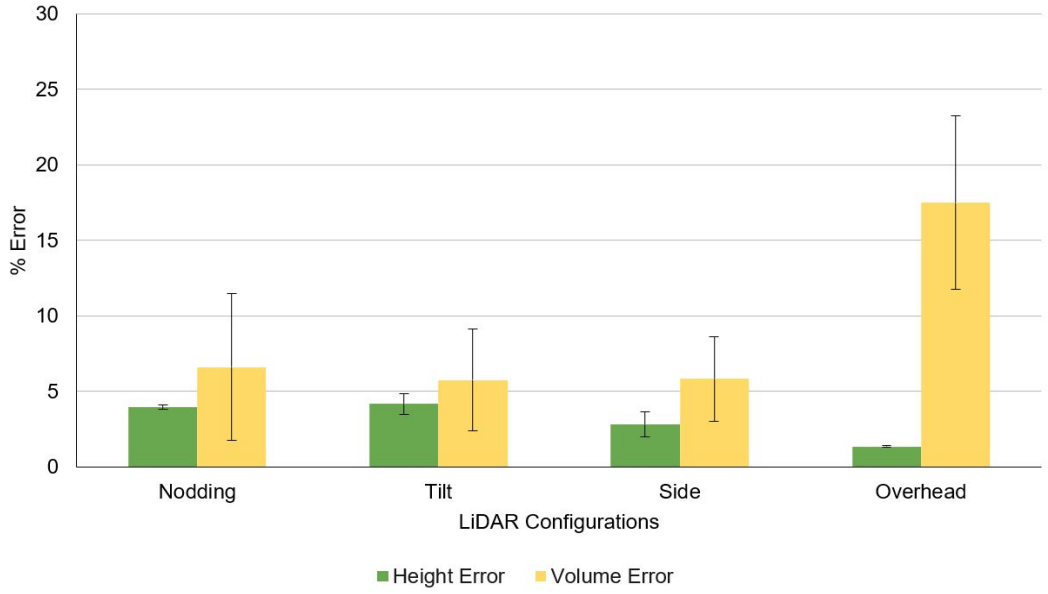

Figure 2.11: Mean percentage error of height and volume phenotyping estimation from four LiDAR configurations. The errors bars indicate the standard deviation.

For plant height prediction, all configurations were able to perform within a low percentage error with an average percentage error of 2.7%. The overhead configuration performed the best with a 1.3% $\pm$ 0.87% average error. This is because a direct overhead angle that obtains a perpendicular-to-the-ground cross section collects more z-axis data from the plot. With this overhead view angle, the LiDAR was better able to characterize the height of the plant relative to the ground because each scan captured the entire top of the crop of interest as well as the ground to the side of the plot. The overhead configuration is more robust in calculating errors for height estimation compared to the tilt (4.2% $\pm$ 0.69%) and nodding (4% $\pm$ 0.14% which are pointed downward obliquely into the crops and does not have a unobstructed view of the ground. In the presence of external error factors such as an uneven ground, the overhead configuration is better able to compensate for height disturbances by more effectively mapping of the ground which was used as the height baseline by the RANSAC algorithm. Height detection using configurations such as side (2.8% is sensitive to bumps and noises, as they have a more limited angle on the z axis cross sections onto the plots. For height estimation all the LiDAR configurations underestimated the height of the cotton plant because the height estimation was an average of the top profile of the attained point cloud data. Additionally the uneven ground has only protruding bumps which elevated the rover and LiDAR, making plant measurements smaller.

Overall this phenotyping study determined that the proposed nodding LiDAR configuration achieves comparable accuracy in volume and height estimation when compared to commonly used configurations

such as side and tilt. The nodding configuration performed height and volume analysis with relatively low error, similar to that of tilt and side. The overhead configuration heavily underestimated volume although it performed height analysis with the lowest error. The main advantage of using the proposed nodding configuration is that while it can be used to phenotype and perform competitively with other commonly used LiDAR configurations, it can also be used for navigation while the other configurations cannot.

Results showed that the navigation strategy performs well in both testing scenarios. In the first scenario where all crop rows were parallel and waypoints were given between each crop plot (As shown by the red circles) (Figure 2.12A) the root mean squared error was 0.0225 m with 32.5 m of travel across three rows, indicating the navigation strategy performed with 0.06% drift from the ideal path. A video of this first navigation test is provided in the supplementary materials. In the second and more challenging scenario, the LiDAR based control algorithm would have to navigate correctly from one plot to the next (Figure 2.12B). In this scenario the root mean squared error was 0.0778 m with 38.8 m of travel resulting in 0.2% drift. Although the performance in the second scenario was less desirable, the navigation strategy overall performed well in both scenarios, achieving well below 1% drift from an ideal path.

Using this navigation strategy, a point cloud of the simulated cotton field was also created (Figure 2.13). This cotton field point cloud could be further analyzed as the phenotyping section of this paper proposed to determine height and volume of each plot. While there could be point cloud errors that were generated due to wheel slippage at way points that required turning, the volume and height estimations were not significantly affected by the navigation course because the "robot_localization" package effectively estimated the pose change from the various localization sensor inputs from the rover and published the appropriate transform to the laser assembler package for combining the LiDAR scans.

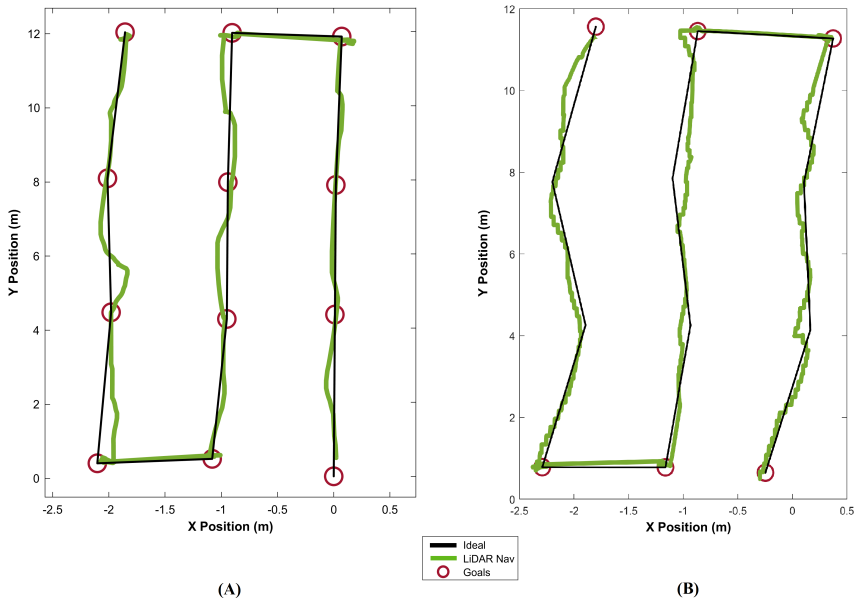

Figure 2.12: Navigation strategy results: (**A**) straight crop rows and (**B**) angled crop rows.

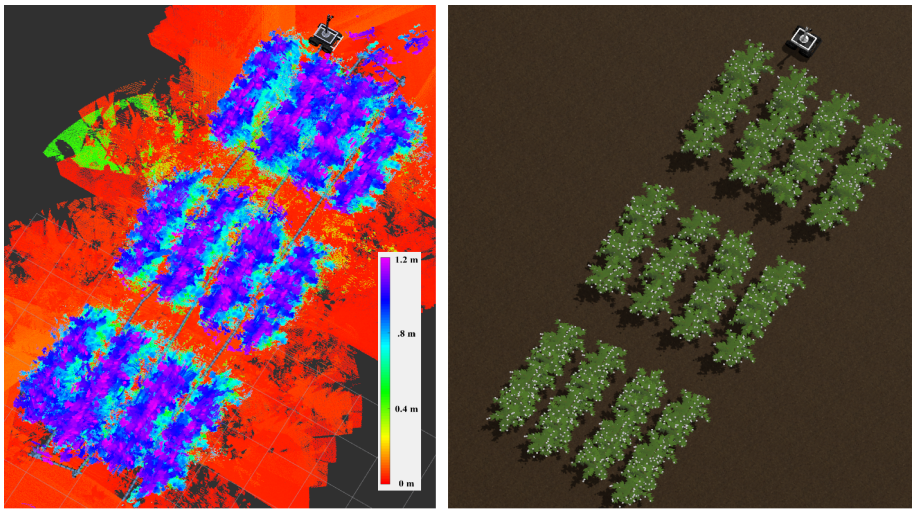

Figure 2.13: (**A**) Generated point cloud of four crop rows and (**B**) the simulation field for navigation tests.

2.3.2 Discussion and Future Work

It was shown through high-fidelity simulation that a nodding LiDAR configuration can be used for simultaneous phenotyping and navigation of cotton crop fields. A simulation approach was used to validate the robot configuration as well as the data analysis procedures.

The use of the nodding LiDAR configuration was validated within simulation by comparing its performance in measuring plant height and volume with other commonly used configurations. The nodding configuration was shown to have low error in estimating the height and volume, similar to that of both tilt and side configurations. This low error is likely due to the nodding LiDAR's ability to "see" the cotton plot from multiple angles while some of the other configurations could not. With the particular volume method used where a hull was formed around the point cloud, having a view of the side profile of the plant greatly increased volume accuracy. Although the overhead configuration performed volume analysis with the most error, it was the most accurate height method because the ground plane was always in view of the LiDAR and was therefore mapped best by this configuration which allowed for better filtering of uneven terrain. However, in total the nodding LiDAR height estimate was only about 2.6% less accurate than the overhead, and with the additional functionality of the nodding LiDAR for navigation, this can be deemed an acceptable trade-off.

The position of the LiDAR unit can heavily influence phenotypic results due to occlusion. For the nodding, tilt and overhead configurations, the LiDAR unit must be above the plot with a certain factor of safety to avoid any branches hitting the LiDAR unit. The side LiDAR configuration is even more sensitive to height placement because if it is too high the underside of the plot will be occluded and if it is too low the topside of the plot will be occluded, consequently affecting the final phenotypic results. Additionally it should be noted that to use the side and overhead LiDAR configuration on a mobile base, two LiDAR units would need to be purchased to perform phenotyping on the left and right crop row.

However with the tilting and nodding configuration, only one LiDAR is needed due to the field of view being large enough to see the left and right crop rows reducing the cost of phenotyping by 100%. This highlights cost effectiveness of the actuated LiDAR because the LiDAR can be used for both left and right crop row phenotyping and navigation.

The errors obtained from this simulation experiment differ from those obtained from a real experiment where plant volume and height was estimated using an overhead LiDAR configuration (Shamshiri, Hameed, Pitonakova, et al., 2018). The RMSE obtained for LiDAR based volume and height estimation was 0.011 m^3 and 0.03 m, respectively in the real-life experiment. Comparatively the best volume and height estimation from the various configurations tested in simulation was 0.0238 m^3 and 0.0071 m. The discrepancy in volume estimation can be attributed to the difference in determining ground truth and different methodology for determining volume. For the real-life experiment, the manual phenotyping measurements were done by measuring the radius of the plant at specific height segments and then combining the volumes of the resulting cylinders whereas due to having the CAD model the ground truth was determined absolutely from the model itself. As such the manual estimation of ground truth using cylinders would be more prone to error and is more of an estimation in comparison to using a CAD model and finding volume directly.

For determining volume in MATLAB, the shrink factor for the convex hull function has a large effect on the volume results of the various LiDAR configurations. For example, the overhead configuration does not capture the underside of the plot and therefore underestimate the volume of the plot. If the shrink factor is decreased, however, the accuracy of the overhead configuration increases. On the contrary, the nodding configuration can capture plant canopy at different levels and its volume estimation accuracy decreases if a lower shrink factor were used.

The simplified cotton plant CAD model has some limitations that may have affected results. The cotton plant model canopy may not have been dense enough to completely block LiDAR scanning from all angles. Typically, cotton plants are dense at late stages of growth, and self-occlusion effects are very prominent. Another aspect that could have affected results was the shape of the cotton plants. The cotton plants modeled had an oval shaped cross section, and plants with different shapes could have resulted in different volume calculations. For example, a pyramidal shaped cross section would have achieved better results from an overhead LiDAR configuration, while a top-heavy plant would yield worse results. This phenotyping study could be advanced further by including plants of different shapes and sizes as well as including plant models of young cotton plants.

A complete navigation strategy that uses both LiDAR for crop row detection and GPS for waypoint following was also developed for the robot that allowed for successful navigation between simulated crop rows with 0.2% error. The navigation strategy however does assume that at each nod both the left and right crop rows are visible to make a valid control action. If both rows are not visible, then the navigation control algorithm fails. Additionally, the LiDAR navigation algorithm may fail if it is not positioned correctly and due to occlusion cannot have a good "view" on the crop rows. The proposed actuated 2D LiDAR-based strategy allowed for the generation of a dense point cloud that made it easier to filter out erroneous LiDAR data, such as hits from branches, by obtaining multiple angular views of the area in

front of the rover and thus a more consistent characterization of the left and right crop rows. This makes the technique less susceptible to occluding factors compared to static 2D LiDAR units, which only view from one angle. By adding multiple levels of functionality to one sensor, the cost of phenotyping and navigation was reduced and the barrier for implementing HTP platforms was lowered. In the future, additional LiDAR-based navigation strategies could be tested with different types of actuation, such as a vertical scanning.

Because of the favorable results of this simulation, the next steps would be to implement this LiDAR-based phenotyping and navigation strategy on real crops to test and compare efficacy with the simulated results. With the ROS implementation of the rover already completed in terms of rover navigation, sensor fusion, as well as LiDAR processing pipeline, the real-life implementation will be quicker due to having prototyped and validated in simulation. However, there are a number of differences between the real life implementation and simulation that will need to be addressed. Localization may have much greater uncertainty in real-life due to many external conditions. GPS may have much greater error or variance due to conditions such as cloudy days, plant occlusion or signal loss. Wheel odometry might show greater slippage or various obstructions such as rocks may cause the rover to move in unpredictable ways. These localization errors will manifest in the LiDAR point cloud generated by the actuated LiDAR, as such additional LiDAR registration techniques may be needed. Additionally in the simulation there was no error associated with the rotation of the LiDAR unit itself, however in real-life there is always some amount of error for actuator positioning which will cause some error with the transform of the actuated LiDAR. An additional source of error is from specular reflectance, when the LiDAR beam is reflected of a surface and result in false positives.

2.4 Conclusions

This paper presents a simulation of a customized mobile platform for autonomous phenotyping that can simultaneously phenotype and navigate through occluded crop rows with the use of a nodding LiDAR. A complete ROS configuration was implemented to represent an agriculture robot for HTP. A high-fidelity simulated cotton crop environment was created as a test bed for phenotyping and navigation strategies. A hybrid navigation strategy that utilizes both a LiDAR-based control algorithm and GPS waypoint navigation was determined to be successful. The simulation methodology presented in this paper will benefit robot development in high throughput phenotyping and precision agriculture.

Chapter 3

Validation of a Multi-Purpose Autonomous Field Robot for Plant Phenotyping and Soil Sensing

3.1 Introduction

The global food supply is threatened by climate change and population growth, but the development of new robust crops can help offset this threat. The development of these crops arise from selective breeding programs where experimental crops are phenotyped and the best variants are selected. Manual phenotyping requires a large labor force and is highly inefficient, which presents an issue known as the phenotyping bottleneck. This bottleneck can be alleviated through the use of agricultural robotics that can perform high-throughput phenotyping (HTP).

Currently, plant breeders cannot measure traits throughout the growing season due to the labor cost of phenotyping. Oftentimes, they measure traits at the end of the season. This limits the amount of data gathered and contributes to the bottleneck, but agriculture robots can autonomously work to gather data throughout the season.

This paper presents a validation of Multipurpose Agricultural Robot for Intelligent Agriculture (MARIA), an autonomous mobile platform that can perform various HTP tasks. MARIA is able to autonomously navigate in both outdoor and indoor settings. An integrated robotic operating system (ROS) is also presented that handles sensor data, localization, and navigation as well as a web based GUI to allow for setting waypoints. Onboard MARIA is an actuated 2D LiDAR that is able to generate point clouds to perform phenotyping analysis such as volume and height estimation. MARIA additionally has a three degree of freedom (DoF) robotic manipulator that can perform geo-located tasks such as measure root zone temperature and humidity and collect soil samples. The onboard manipulator also has an interchangeable end effector allowing for different functionalities which is demonstrated with a soil

sampling end effector design. MARIA is unique in that the platform is re-configurable to work with other autonomous systems extrusion based design and use of off-the-shelf components and 3D prints. As such, it has the potential to be more widely available for use for HTP work as the designs are able to be replicated/modified.

3.1.1 Related Work

Mobile Robots for Phenotyping

With an autonomous robot, plant traits can be measured throughout the entire growing season allowing for greater data collection and more effective plant breeding and analysis. Novel autonomous mobile platforms have been developed such as "The Robotanist," a ground-based robot able to autonomously navigate sorghum and corn crop rows as well as deploy a wide range of phenotyping sensors such as LiDAR and cameras to gather sub-canopy data (Mueller-Sim et al., 2017). Another robot architecture for plant phenotyping was also presented with the "Vinobot and Vinoculer" in which a mobile ground platform (Vinobot) for individual plant inspection was paired with a mobile observation tower (Vinoculer) for overseeing an entire field (Shafiekhani et al., 2017). A low cost, 3-D printed rover, the "TerraSentia," has also been developed as an ultracompact, lightweight solution for autonomous phenotyping(Kayacan et al., 2018).

Large scale robots have been developed for high throughput phenotyping such as BoniRob, a four wheel steering robot (Ruckelshausen et al., 2009), and Thorvald where modular drive components could be reconfigured to form different drive systems (Grimstad & From, 2017). An open source tracked robotic system was proposed using using off the shelf components to perform sub canopy plant phenotyping (Stager et al., 2019).

LiDAR Phenotyping

Light Detecting and Ranging (LiDAR) sensors are one of the most widely used sensor systems in robotic platforms because of their ability to give accurate distance measurements without contact. LiDAR is increasingly being used in the field to generate 3D point clouds of crops for phenotypic analysis (Wang et al., 2017b) as well as low-cost crop navigation (Pabuayon et al., 2019b). With a 2D LiDAR, point clouds are able to be generated to determine important phenotypic traits of plants, such as canopy height and plant volume (Sun et al., 2018b).

LiDAR has been used extensively on robotic mobile platforms for high-throughput phenotyping by statically mounting the 2D LiDAR on a mobile platform and moving it directly overhead or to the side of the ground plant (Jimenez-Berni, Deery, Rozas-Larraondo, Condon, et al., 2018; Llop et al., 2016b; Sun et al., 2018b; Wang et al., 2017b; White et al., 2012b). A low cost method of generating a 3D point cloud with a 2D LiDAR is to mount the LiDAR on a servo motor such that it "nods" back and forth to generate a 3D point cloud (Harchowdhury et al., 2018b).

Navigation is another common application of 2D LiDAR as a way to allow mobile ground robots to map crop rows and therefore navigate reliably (Malavazi et al., 2018a). GPS guided navigation is also

typically used for field robots and allows for waypoint following in agriculture settings, but does not conduct active obstacle avoidance .

Soil Sensing and Robotics

Another important aspect of sustainable agriculture and phenotyping is characterization of soil properties such as moisture content and temperature. Phenotyping of root traits for drought resilient genotypes (Passioura, 2012) is an area of particular interest due to climate change. Measuring changes in moisture content in soil gives important information on plant water-uptake rates, as well as estimating parameters such as rooting depth (Bitella et al., 2014). Soil temperature is also an important quantitative measure as temperature affects root growth and architectural traits (Nakamoto, 1995). Root zone temperature has an impact on stressors such as salinity (He et al., 2014) and pathogen infection rates (Watt et al., 2006). Soil hydraulic properties have spatial correlation ranging between 10 to 20 meters, with such variability a high number of sensing nodes in an agricultural field would be needed.

One solution to the cost of having a large amount of instrumentation is to use robots to perform these soil sensing tasks at target locations, such as a six-wheeled robot with an "e-nose" that consists of an array of six gas sensors for the detection of organic volatile compounds (Pobkrut & Kerdcharoen, 2014).

Additional uses of mobile robotics have been found in the scope of soil sampling which is traditionally done manually. Bonirob, a commercial four wheel steering agriculture robot was fitted with a soil penetrometer for measurement of soil compaction (Scholz et al., 2014). An additional six-wheel platform was developed to be able to take soil measurements (Łukowska et al., 2019) inspired by space rovers.

Mobile Robotic Manipulators

In the agriculture environment, manipulators are commonly added to mobile robots to automate traditionally manual tasks. This greatly increases agricultural efficiency as mobile robots are able to work continuously and at low costs. Weeding is one common manipulator task done by mobile robots (Van Der Weide et al., 2008). In one example, a manipulator mechanically uproots a weed (Åstrand & Baerveldt, 2002). In other examples, actuators spray herbicide at a target location (Gonzalez-de-Santos et al., 2017) such as Ladybird, a solar powered mobile robot that has a robot arm with a herbicide spray end effector (Bogue, 2016). Servo-based actuators have also been developed and added to a mobile robot to perform seeding in the field (Hassan et al., 2016). A mobile robot was developed with a two DoF parallel robot arm manipulator for handling paper pot seedlings (Rahul et al., 2019). Robots have also been developed to mechanically evaluate crop fields using manipulators such as Robotanist that deployed a manipulator on a mobile robot to measure stalk strength (Mueller-Sim et al., 2017) or BoniRob a four wheel steering robot to measure soil compaction (Scholz et al., 2014). A prototype mobile manipulator for agriculture was proposed for general purpose use in an agricultural environment (Bascetta et al., 2017).

Gap/Motivation

There has been extensive research on the development of autonomous, HTP robots, but there still exist several gaps in the current work. Most designs require custom fabrication and are not available for commercial purchase, which limits their use in the field, but this work presents a system that can easily be replicated and modified through use of off-the-shelf or 3D printed components. Additionally, many of the HTP systems do not allow for both phenotyping with LiDAR and soil sensing as this work does. This work also allows for the mobile actuator to be reconfigured to fit specific needs through the use of Dynamixel servos and a new open source library.

3.2 System development

MARIA is an autonomous differential drive rover with various phenotyping sensors and a three DoF manipulator (Figure 3.1). The main computational system on board the MARIA rover is a Jetson Nano (Jetson Nano, Nvidia, California, United States of America) running Ubuntu 18.01 with Robot Operating System (ROS Melodic).

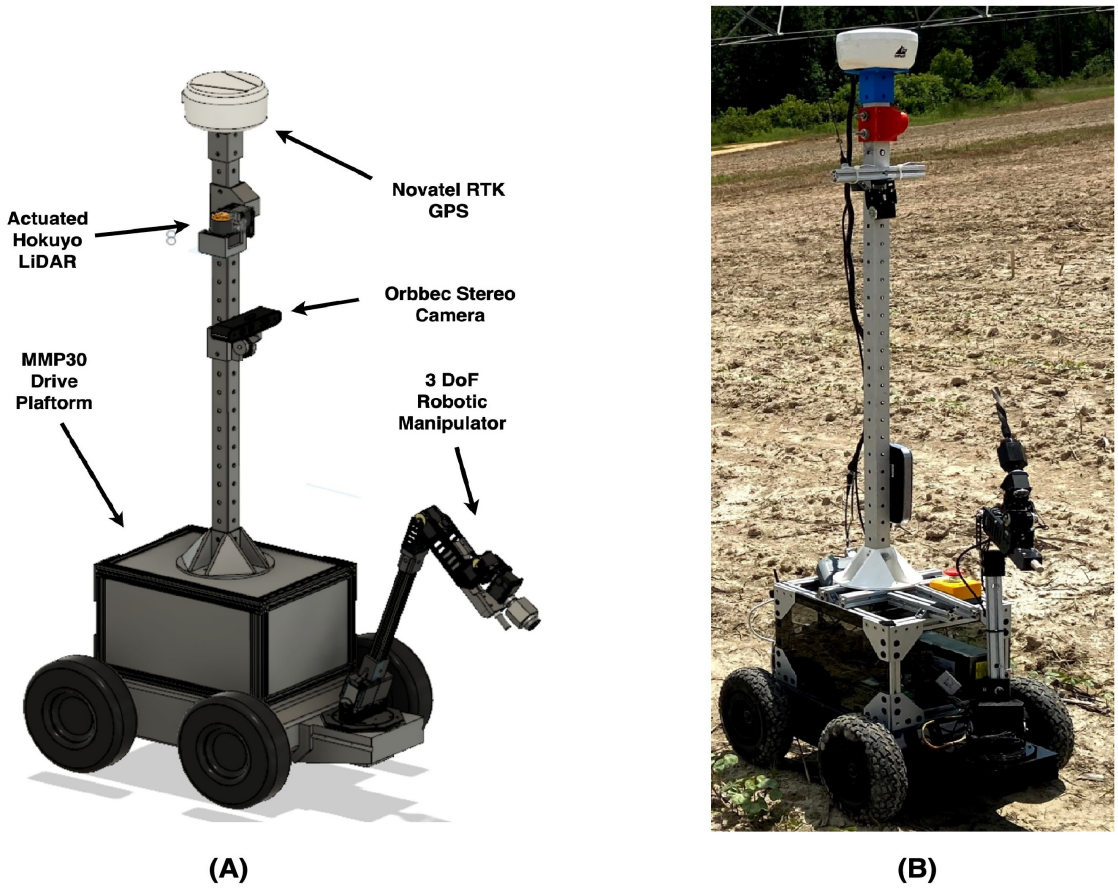

Figure 3.1: (A): CAD model of MARIA (B): Picture of MARIA

3.2.1 Autonomous Drive System

Drive System

The MARIA base consists of the chassis and drive system and is sourced from The Machine Lab (MMP30, The Machine Lab, Fort Collins, Colorado). The MARIA has an extrusion based framing on top of the base which allows for an easily configurable and modular system for installing a variety of sensors and other components. The platform is equipped with two 25V NiCad battery packs in parallel, with a total run time of approximately one hour at peak use. Each motor controller controls two, 24 V DC servo Gearmotors with a stall torque of 860 Oz-in. Each motor is fitted with an optical encoder (HEDS 9100, Broadcom, California, USA) that has a resolution of 500 counts per revolution (CPR). With a total gear reduction of 46:1 the total encoder measurement accuracy for rotation is .0156 degrees. The motor control system consists of two, 2x12 sabertooth motor controllers which are connected to a motor driver (Kangaroo, Dimension Engineering, Ohio,USA). The Kangaroo motor driver has a built in PID (proportional, integral, derivative) controller which can tune itself based on encoder information. The Kangaroo motor driver in turn communicates directly to the onboard single board computer (SBC)

through a USB-TTL converter. The Kangaroo motor driver is communicated through packetized serial and the arduino libraries provided by Dimension Engineering.

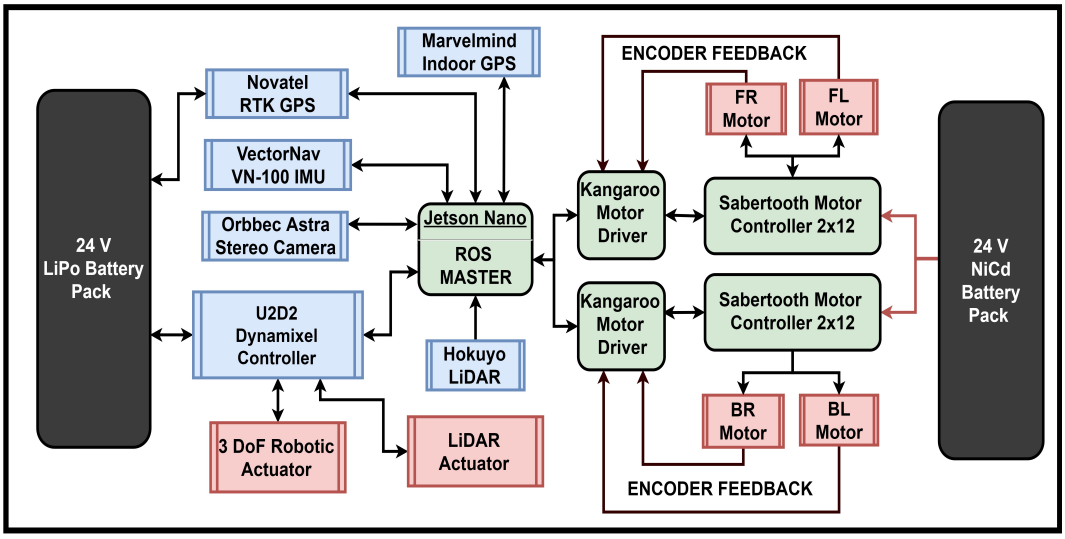

Figure 3.2: Block Diagram for MARIA

Localization

Multiple sensors were used for localization of the rover in an inertial frame. Wheel odometry was calculated using the wheel encoder feedback of the left and right DC motors. An inertial measurement unit (IMU) (VN-100,Vectornav,Texas,USA) was used for measuring acceleration as well as heading. For global positioning two different sensor units were utilized. For localization in an outdoors environment a real time kinematic (RTK) Global Navigation Satellite system was used (SMART6-L,Novatel,Calgary,Canada) . For an indoors environment a relative global positioning system was implemented (Marvelmind Indoor GPS,Marvelmind,Tallinn,Estonia) . Marvelmind indoor GPS uses a set of stationary and mobile beacons that use ultrasonic signals to localization relative to each other using trilateration. These various localization signals were then input into an extended kalman filter which allows for sensor fusion and output an accurate pose in a global environment. The extended kalman filter was implemented through the robot_localization package ("robot_localization", n.d.) . The robot_localization package allows for arbitrary input of various localization sources into a kalman filter as well as publish various transforms to the ROS tf library. The ROS transform library creates a transform tree from the map frame down to the robots base frame.

A calibration step is required for fusion of heading of the IMU and the heading using a global position system such as GPS or the Marvelmind beacons. This is due to the IMU measuring heading by detecting magnetic north which can be distorted by various surrounding magnetic sources while the global positioning system is not as sensitive. As such there is an offset needed to align the heading of the IMU and the heading of the global positioning system. This is done by calculating heading in the global system by measuring two points to calculate a line and angle. The difference between the global positioning heading

angle and the IMU is then applied to the IMU. The global position heading calculation using Global Navigation Satellite systems requires using UTM coordinates which is defined by dividing the earth into respective square zones. Within these zones, Euclidean geometry is valid by assuming flatness.

GPS based navigation was implemented for the MARIA using the gps_common package and navigation stack. Firstly the correct transforms had to be implemented to convert GPS goals in longitude/ latitude into the MARIAs's frame of reference as latitude/ longitude coordinates are defined in non-Euclidean space making it difficult for use in autonomous navigation. For this purpose, the GPS_common node takes in latitude/ longitude and outputs UTM coordinates. UTM coordinates are defined by dividing the Earth into respective square "zones". Within these zones, Euclidean geometry is valid by assuming flatness. One necessary step for autonomous navigation using GPS based waypoint navigation is the reconciliation of the UTM heading and the IMU heading. These two headings need to be aligned otherwise these two localization components will conflict with each other and give incorrect heading results when Kalman Filter sensor fusion is performed. This discrepancy between the UTM heading and the IMU heading is caused by distortion of the surrounding magnetic field. This distortion causes the IMU heading to have a yaw offset. To compensate for this, a "yaw offset" is applied by measuring the angle between two UTM points and then the yaw value from the IMU. Then the difference between the UTM angle and the IMU yaw is applied resulting in the necessary offset needed to align the UTM frame and the IMU frame. A calibration procedure was programmed to use the mmp30's frame at two different UTM points (converted from GPS points using gps_common ROS package) to find the difference between the angle from the easting axis and the yaw from the IMU sensor. This yaw offset was applied to all the IMU angle readings before being published to the /imu/data topic.

The MARIA is also compatible with the MarvelMind indoor GPS system for time of flight (ToF) based localization, which is useful for indoor applications such as greenhouses. This indoor navigation with absolute positioning is based off of absolute global positions from ultrasonic beacons using the MarvelMind Indoor GPS. The indoor GPS beacons are able to get their relative positions from other beacons using ToF calculations of ultrasonic clicks. With these relative positions, a map is created. A mobile beacon (also called "hedgehog") sits on the rover and has a mobile position with the origin designated at one of the stationary beacons. Marvelmind has a ROS package that enables the position of the mobile beacon to be published as a ROS topic. However for this global pose estimate to be fused with the robot_localization package, a publisher/subscriber node has to be created to adapt the raw position value into the nav_msgs/Odometry message.

Path Planning

Pure pursuits was implemented as the planner of choice for the MARIA due to its simplicity and robust performance. Pure pursuits is a tracking algorithm developed in the 1980's for calculating a curvature needed to get to a specific point. (Figure 3.3) illustrates the Pure Pursuits geometry. Pure pursuits geometrically calculates curvature needed to get to a specific point that is determined from a "look ahead" coordinate. The look ahead coordinate (x,y) is a point on the desired path that is a "look ahead" distance

away from the rover. A vector L is defined from origin to the look ahead coordinate. Using trigonometry these following equations can be defined:

From these equations 3.1 the curvature that the robot has to follow to reach the look ahead coordinate can be determined. As the robot moves, the curvature is continuously recalculated as the look ahead point is continuously updated at a distance L. The robot is essentially continuously pursuing this point by following some curvature.

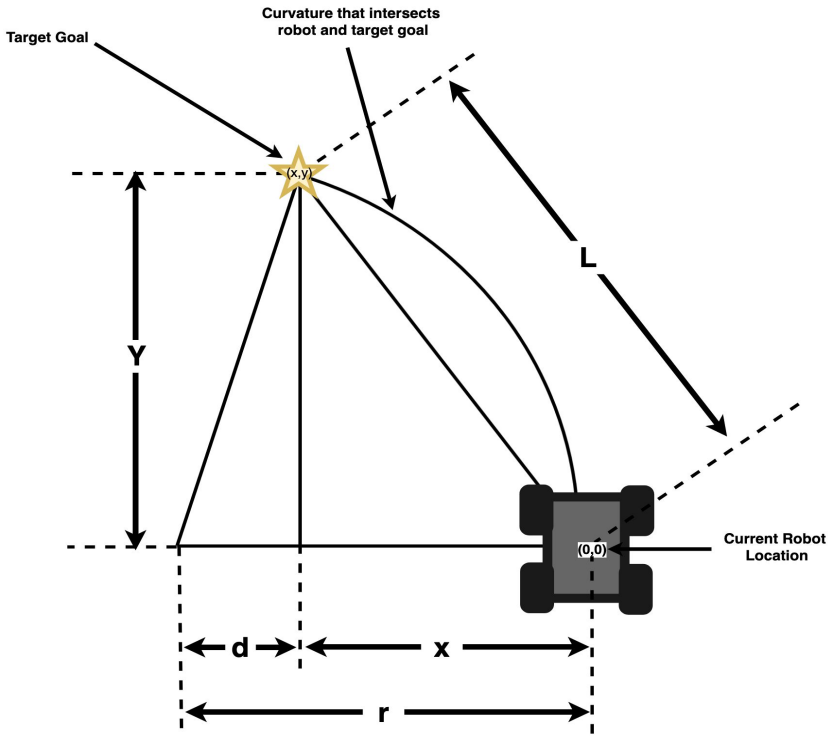

Figure 3.3: Geometric Relationships for Pure Pursuits

$$x^2 + y^2 = L^2 \tag{3.1}$$

$$x + d = r \tag{3.2}$$

$$(r - d)^2 + y^2 = L^2 \tag{3.3}$$

$$r^2 - 2rx + x^2 + y^2 = r^2 \tag{3.4}$$

$$2rx = L^2 \tag{3.5}$$

$$r = \frac{L^2}{3x} \tag{3.6}$$

3.2.2 ROS Framework / Simulation

Robot Operating System (ROS) was used as the central framework for data communication between all of MARIA's subprocesses. One of the major sub processes is the autonomous driving capability. First this starts with localization where for each sensor a node is started to publish to the appropriate topic (Figure 3.4). This is used as input to the robot localization ROS node that uses an extended kalman filter to output a state estimate. The next major subprocess in the drive node. This takes feedback from the Kangaroo motor controllers on the rotation of the left and right wheels and then outputs them into the Diff-Drive node. The Diff-Drive node is used to calculate and publish odometry as well as accept velocity commands, translated from an overall velocity of the robot to the velocities of the left and right wheels. UART is used through the U2D2 to control the Dynamixel servos (Dynamixel Smart Servos,Robotis,Seoul,South Korea) which are used in both the onboard three DoF manipulators as well as for actuating a LiDAR unit. For managing autonomous navigation a move_base node was created. Move_base node is an implementation of the ROS navigation stack which allows a standardized interface to control the robot as well as have feedback with a path planner of choice. The move_base node then outputs command velocity topics to reach its goal based on its current location/status. The move_base node outputs a velocity command directly to the Diff-Drive node which in turn sends right and left wheel velocities to go the desired trajectory.

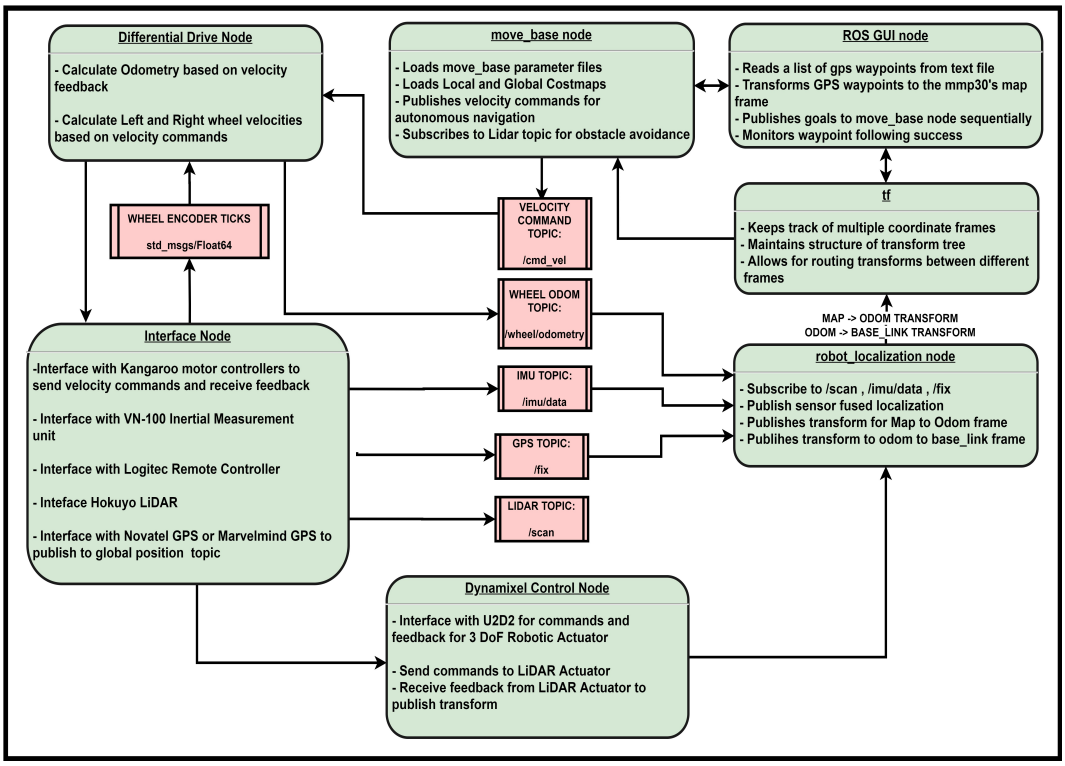

Figure 3.4: Simplified ROS Node Diagram

For high level control a Graphic User Interface (GUI) was added which provides a 3D rviz-like window to visualize the URDF, odometry heading, and present location of the robot in its TF 'world_frame'.The GUI utilizes ROS, the HTML/CSS/JavaScript web stack, roslib.js, ros3d.js and the Apache web server (Appendix III) to provide an intuitive interface to send position commands for robots in the field. The window is accompanied by a small amount of additional telemetry (odometry) as well as some interactive elements to control various parts of the client. Upon accessing the web page, the user can enter the IP address of the robot they wish to connect to, and select the odometry topic they wish to use for visualization from the drop down menu. Once the robot is connected, they can use the 'Capture Position', 'Clear Markers', and 'Move to Markers' buttons to capture and display an odometry waypoint, clear existing odometry waypoints, or move the robot to existing odometry waypoints in the order they were captured.

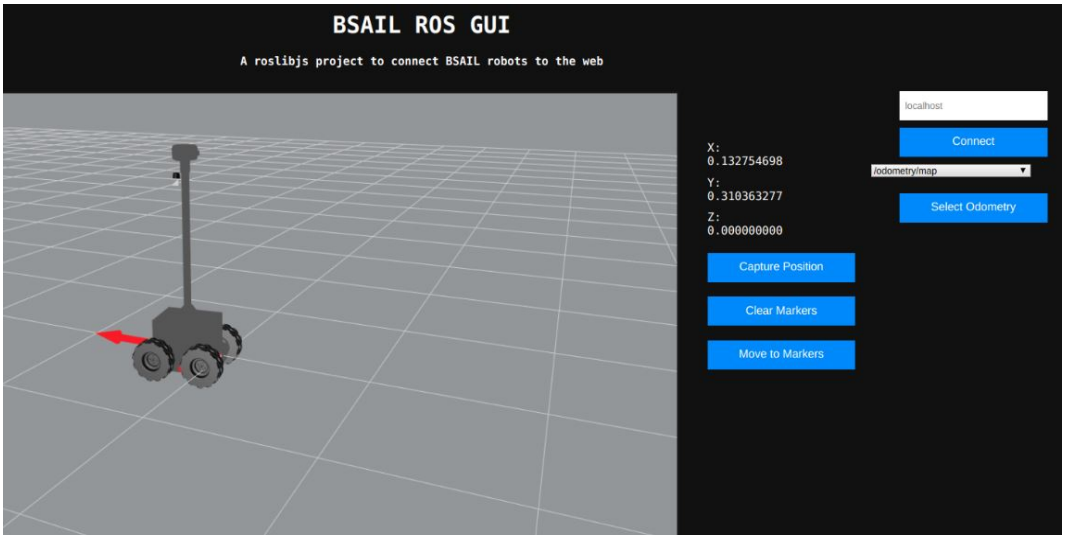

Figure 3.5: GUI Interface for MARIA

For prototyping and testing of the ROS system a simulation twin was created of MARIA using Gazebo (Figure 3.6 A), a physics simulator, and ROS as the data communication interface. This simulation adds to the author's previous work with the addition of a three DoF manipulator. A Universal Robot Description File (URDF) was generated from solidworks using the solidworks to URDF plugin. And then revolute joints were added for the wheels and the manipulator joints. Using the URDF of the manipulator a ROS package called MoveIT was used to generate a moveit package that allows for interfacing with the manipulator as well as visualizing manipulator movement (Figure 3.6 B).

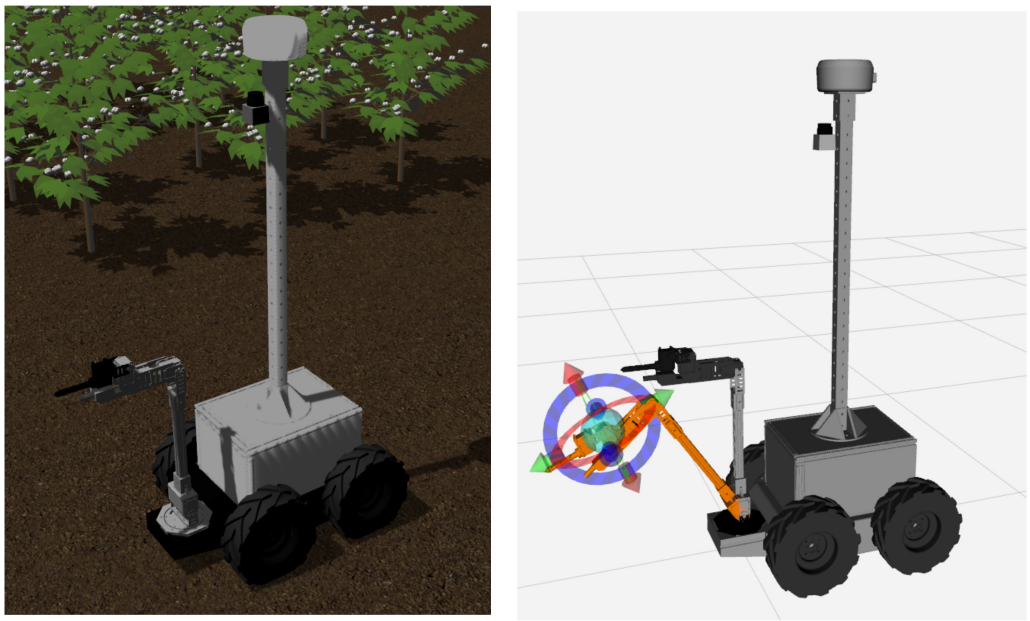

Figure 3.6: Gazebo Simulation (A) , Moveit! RVIZ Visualizer (B)

3.2.3 Mobile Manipulator

A three DoF actuator was developed using 3D printed joint connecters and the links being made of extrusion (Figure 3.7). The joints are designed to allow for different length extrusions to be connected, allowing for customization of the workspace of the onboard manipulator

Figure 3.7: CAD model of manipulator

Multi-Purpose ToolHead

A toolhead was created for the Dynamixel end effector to allow the changing of different end effectors. The toolhead changer was inspired by the same mechanism as an electric screwdriver chuck where it is necessary to hold different tools and provide rotational force. The chuck functions through use of a rotational motion from the shaft that pushes the jaws forward and around different bits (Figure 3.8). For the jaws of the chuck to move around or out of a bit, the outside of the chuck has to be stationary, as such the outer case was made into an hexagonal shape. When the chuck is put into a hexagonal shaped tool changer, the outer case locks and allows the jaws to be positioned and grab onto the bit of the desired end effector

Various tool heads were designed and 3D printed to validate the tool head changing capability of the robotic manipulator. One end effector was a drill to penetrate soil and allow for the insertion of a

temperature and humidity probe that is later detailed in this paper. A prototype soil sampling cartridge was also designed with the ability to be picked up with the end tool head changer and then be rotated into the soil. At the end of the cartridge there are angled jaws that scrape the soil and then through the downward pressure of the cartridge exerted by the robotic manipulator the loosened soil pushes into the cartridge as it rotates. Once rotated down to a sufficient degree, the soil is compacted into the opening enough to keep the soil well lodged in the cartridge, a video of this process is provided . Additionally the soil cartridge has a screw top opening allowing for easy opening to access gathered soil as well as for wash and reuse.

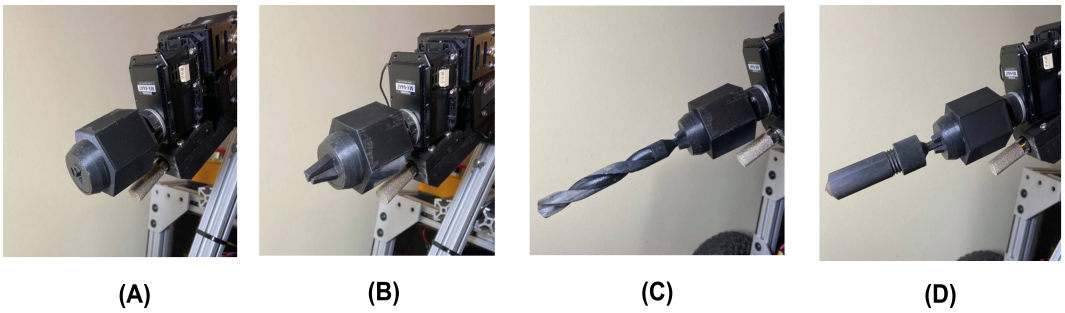

Figure 3.8: Multipurpose Tool Head (A) Tool head with jaws retracted (B) Tool head with jaws extended, (C) Tool Head with a soil drill bit , (D) Tool head with soil sampler)

Hardware

The Dynamixel servos by Robotis was used for actuation of the joints. Dynamixels are a series of smart motors used extensively in this study's robot system for actuation of both the onboard robotic manipulator and the Hokuyo LiDAR. They provide an ability to daisy-chain motors into a serial connection for convenient wiring of complex systems without requiring complex electrical harnesses to utilize many motors in robotic systems. Dynamixel motors use a UART serial data connection to send values to an internal control table allowing for velocity and position control as well as feedback from internal sensors such as current. However when using multiple Dynamixel motors of different models, some of the older models use different protocols for sending commands to the servo's control table. The control-table addresses the need to be specifically managed for each type of motor, causing difficulty implementing a hybrid system. For the purposes of solving this issue, a library was written alongside the overall system to implement an object-oriented method of communicating with many Dynamixel motors of any model rather than interfacing with the raw data values. Each individual motor is treated as an object of a generic motor, which has details of the motor populated as internal variables and functions depending on the motor requested. Each detail of the motor is stored as a JSON configuration for each possible motor using a Dynamixel protocol. By storing each address with its corresponding variable name as a string, similarities between the motors can be used to set motor parameters according to the name of the value desired to be viewed or modified rather than interfacing with an platform-dependant address value. For the most common motor usages, this library provides added functionality of specific functions for setting

and reading values to achieve a desired goal rather than even setting based on name, which is useful in situations of upgrading a motor between generations where the Dynamixel family began to use new naming conventions. Other differences exist between the two generations which needed to be accounted for. The most prominent being that the Protocol 1.0 motors, the older generation, use 1's complement encoding of negative numbers while Protocol 2.0 and most computers use 2's complement.

Kinematics

The analytical solution for the inverse kinematic equations for a 3 DoF articulated manipulator is presented (Figure 3.9). A general equation is proved due to the lengths of the robot arm being made of extrusion, it is possible to have various length configurations for the links L_1 and L_2.

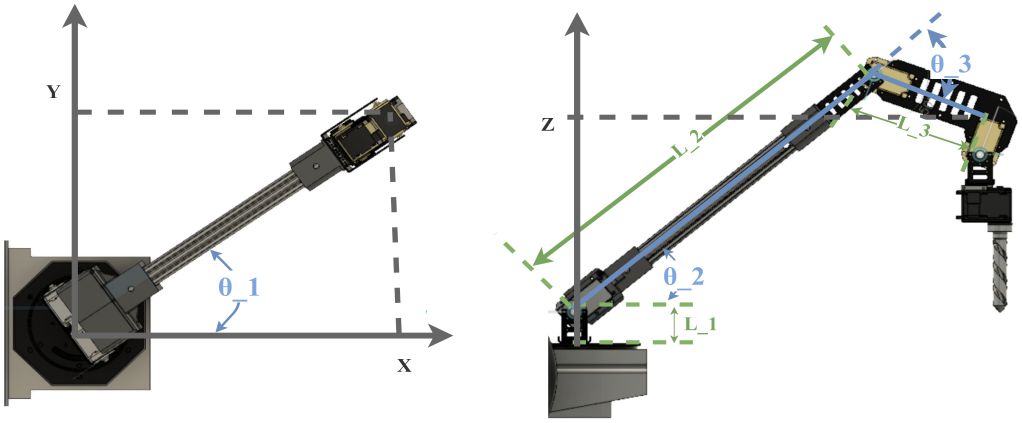

Figure 3.9: Geometric Relationships for Inverse Kinematics

$$\theta_1 = atan2(\frac{y}{x}) \tag{3.7}$$

$$a = \frac{x^2 + y^2 + (z - L_1)^2 - {L_2}^2 - {L_3}^2}{2L_2L_3} \tag{3.8}$$

$$b = +\sqrt{1 - a^2} \tag{3.9}$$

$$\theta_3 = atan2(\frac{b}{a}) \tag{3.10}$$

$$\theta_2 = atan2(z - L_1, \sqrt{x^2 + y^2}) - atan2(L_3b, L_2 + L_3a) \tag{3.11}$$

3.2.4 Phenotyping

Non-Contact Sensors

One of the phenotyping sensors on MARIA is an actuated Hokuyo UST-10 LiDAR. This 2D LiDAR is actuated in a 50 degree range around its y-axis as seen from (Figure 3.10). While the LiDAR unit is actuated the feedback from the Dynamixel servo is used to apply a transform using the ROS transform library. This transform allows a 3D point cloud of the environment to be generated .

An additional non-contact sensor onboard MARIA is an Orbbec stereo camera. Which through stereo vision allows for generating depth clouds. These depth clouds could be used for volume estimation of crops. The Orbbec stereo camera is also able to take RGB images of target areas.

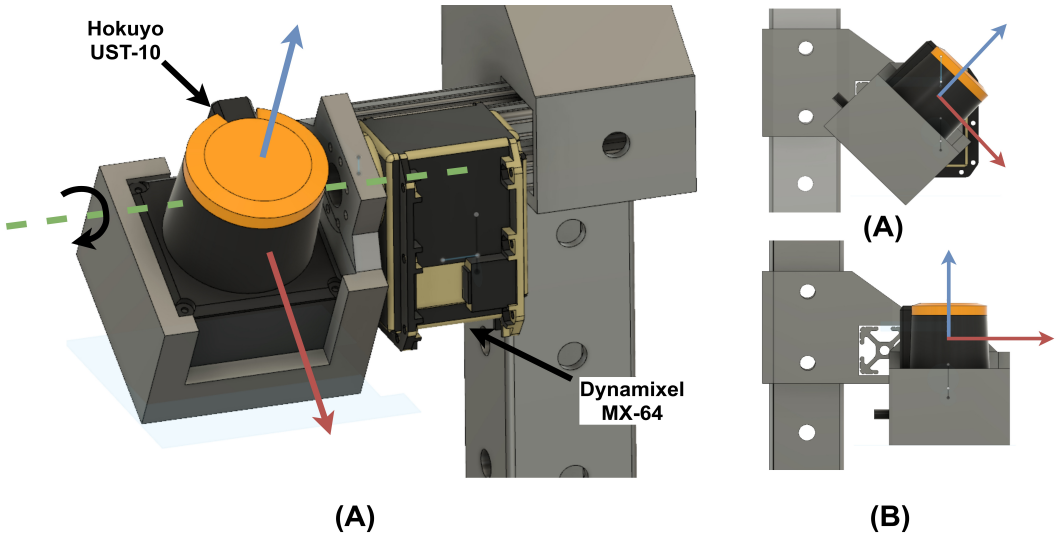

Figure 3.10: Actuated LiDAR Setup

Soil Sensing

For soil sensing, a drill with an end bit was designed and coupled with a temperature/humidity sensor probe onboard the robot arm. The robotic arm first drills to a certain depth (Figure 3.16 A-B) and then inserts a temperature and humidity probe into the soil (Figure 3.16 C-D). This allows for root zone temperature and humidity measurements. The drill and probe are able to penetrate up to four inches into the soil.

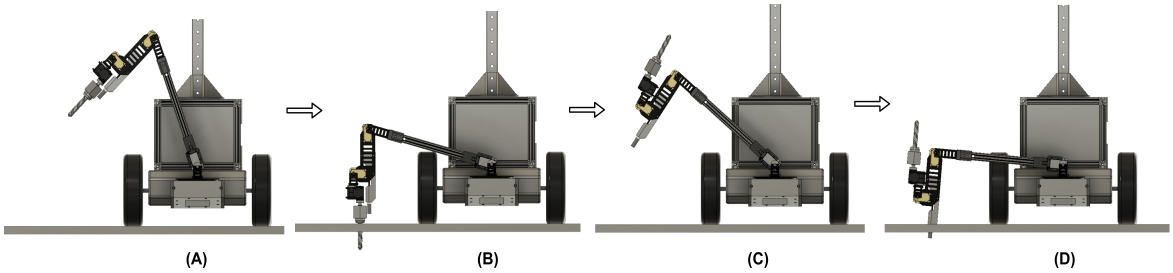

Figure 3.11: Soil Sensing Procedure (A) - (B): Drill Deploying and Drilling into Soil , (C)-(D) Soil Sensor Entering the Soil to take Temperature and Humidity Measurement

3.3 Results

3.3.1 Navigation Results

Navigation was performed outdoors with two different global localization sensors. For the first global positioning system, the Marvelmind ultrasonic beacons were used and mounted on posts around the robot (Figure 3.12 A)

The robot was given four global waypoints to navigate to. The RMSE for marvelmind beacon based navigation was 0.1566 m (Figure 3.12 B). The second localization method used was using the SMART-6 Novatel RTK GPS. The RTK GPS based navigation resulted in a RMSE of 0.2692 m (Figure 3.12 C.

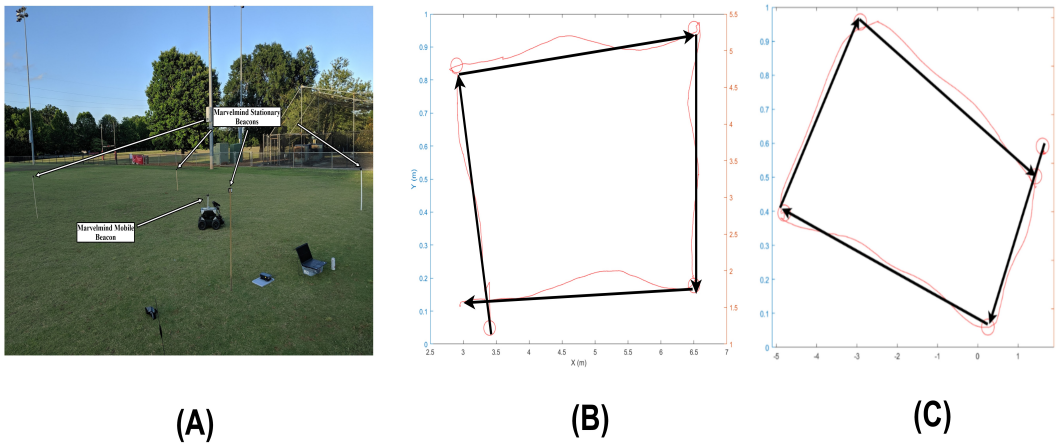

Figure 3.12: Navigation Results (A): Marvelmind based Navigation setup (B): Marvemind Beacon Navigation (C): RTK Novatel GPS Navigation

3.3.2 Non Contact Phenotyping Results

For validation of the phenotyping capability of the actuated LiDAR configuration for MARIA, five plants of various sizes were placed in a line while the rover drove parallel to the plants collecting point cloud data 3.13

(A)

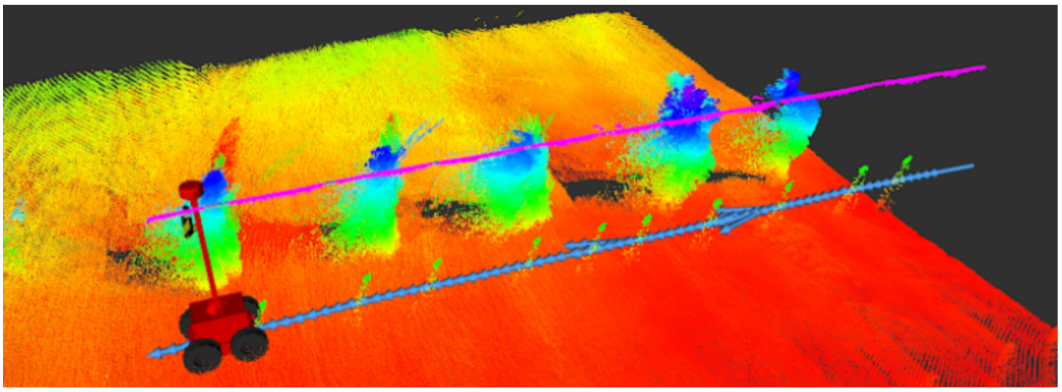

(B)

Figure 3.13: LiDAR Testing Setup

The volume of a cylinder was calculated for each increment and aggregated to estimate the volume of the plant. For the LiDAR validation experiment the actuated LiDAR rotated 50 degrees in 5 seconds allowing for a full "nod" period of 10 seconds. MARIA was moved at a velocity of 0.1 m/s parallel to the row of plants. The point cloud was generated from the laser scan using the laser_assembler ROS package and then post processed in MATLAB 3.15 B). Within MATLAB the volume was ascertained using the convex hull function with a shrink factor of 0. The resultant volume estimation was then scaled by a factor of 4 due to the underestimation from limited view from the point cloud generated by LiDAR. The ground truth for the volume of the plants was determined manually by measuring the width of the plants at multiple increments along the height of the plant. The resulting volume estimation had $R\hat{2}$ of 0.989, a RMSE 0.0435 and an average percentage error of 1.76

Another phenotypic ability that was analyzed was the ability to measure height. For height measurement a RANSAC algorithm was used to measure the ground plane. Then the point cloud was analyzed to find the highest point and its height relative to the ground plane. Using this height method, the proposed strategy had an R2 of 0.984, a RMSE of 0.068 and an average percentage error of 3.2

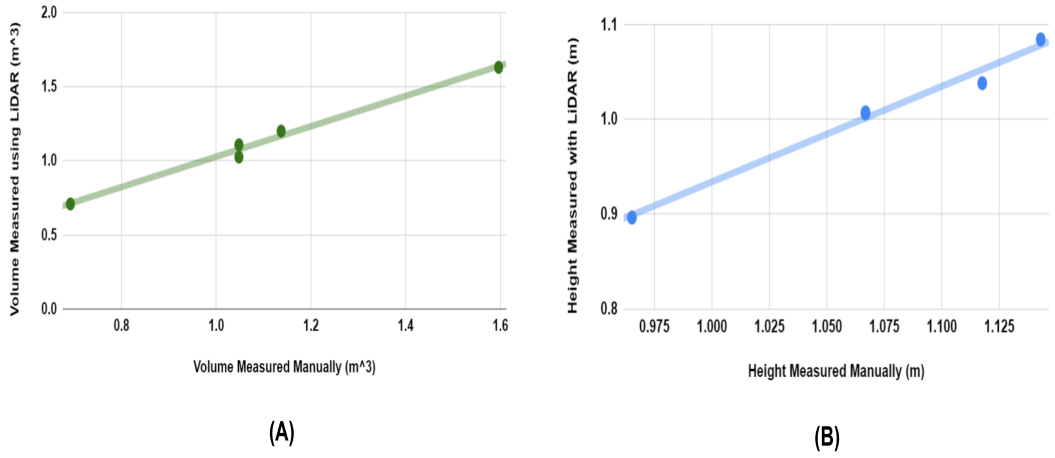

Figure 3.14: LiDAR Phenotyping Results (A): Volume Estimation (B): Height Estimation

The ability of the onboard non-contact sensors were tested and show ability to gather data on different spectrums. Stereo camera is able to construct a depth image as well as take a RGB image, while the actuated liDAR is able to generate a point cloud.

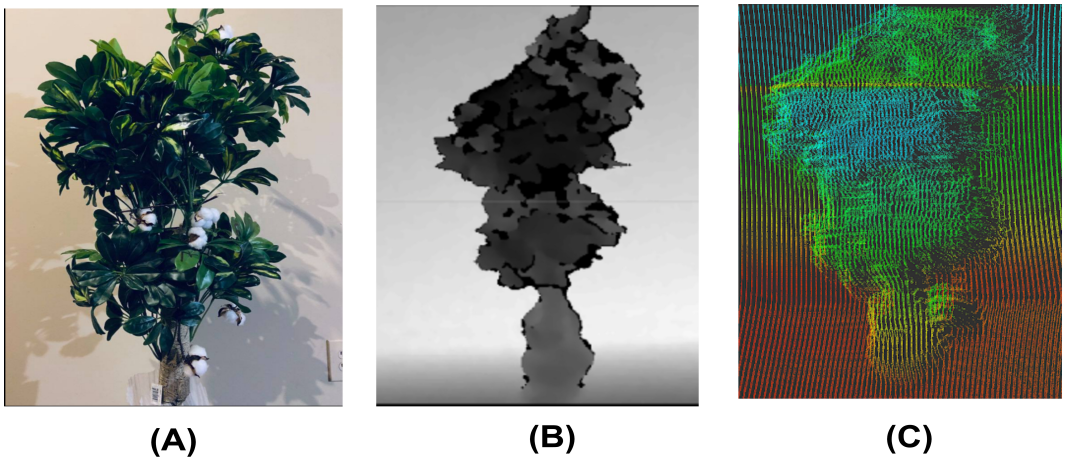

Figure 3.15: Non-Contact Sensing (A): RGB Image (B): Stereo Image (C): LiDAR Pointcloud

3.3.3 Soil Sensing

The soil sensing capability of the onboard robotic manipulator was tested in a controlled soil setting by first shining a lamp on a soil pot for two hours and then having the robotic arm collect temperature and

moisture data at five data points at approximately two inch increments along the pot plant (Figure 3.16). The temperature and moisture probe was able to measure the positive temperature and negative moisture change along the pot plant due to being exposed to a heat lamp. Based on a line fit R$\hat{2}$ value 0.908, the rate of change of the temperature was 0.515 degrees Fahrenheit per inch. For moisture change a line fit R$\hat{2}$ value 0.905 was attained and an estimated moisture change of -3.6 % per inch.

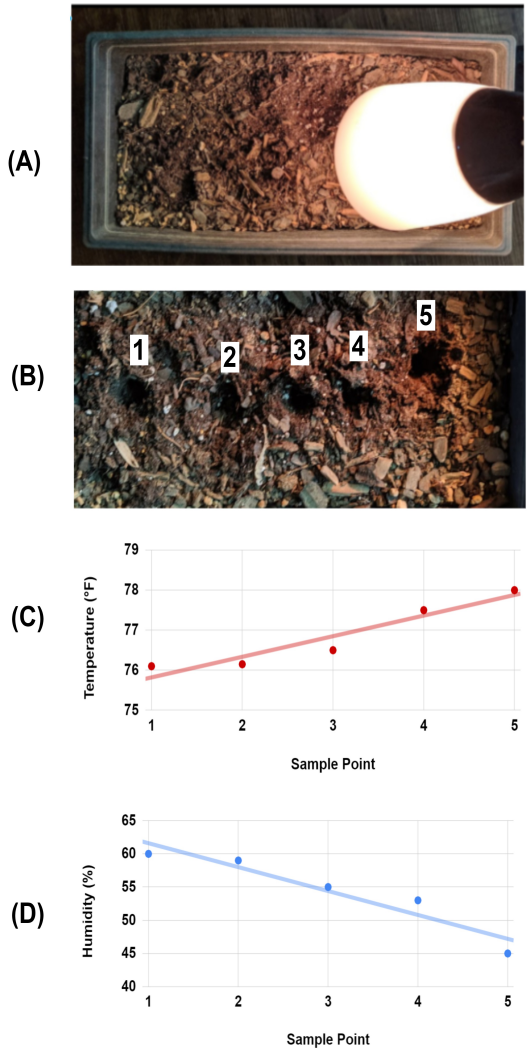

Figure 3.16: Soil Sensing Setup (A): Soil Conditioning with Lamp , (B) Soil Measurements Locations (C) Temperature Measurements, (D): Moisture Measurements

Lastly, a test was conducted to assess the ability of MARIA to combine global navigation and soil sensing by commanding MARIA to move to a specific global waypoint and then use the mobile actuator to drill and insert the temperature and humidity probe into a pot filled with soil. Video of these tests are available. The four soil pots were put into multiple configurations such as a square (Figure 3.17 A), a straight line (Figure 3.17 B), and a random, unstructured configuration (Figure 3.17 C). Waypoints were

Table 3.1: Results of Navigation and Soil Sensing Test

Setup	Number of Targets	Average Time Taken per Pot (seconds)	Manipulator Action Success Ratio
Square	4	62	1
Straight	4	45	1
Random	4	70	.75

determined by driving the rover to a specific position and recording its position and heading. Each pot was six inches in diameter resulting in 28.3 in^2 area for the manipulator to drill and insert probe. One test was conducted for each of the configurations. MARIA was able to gather data with 100% success for configurations (Figure 3.17 A and B) however for configuration (Figure 3.17 C)the manipulator was unsuccessful in sensing one of the four potted plants resulting in an average success rate of 91.7% for all tests.

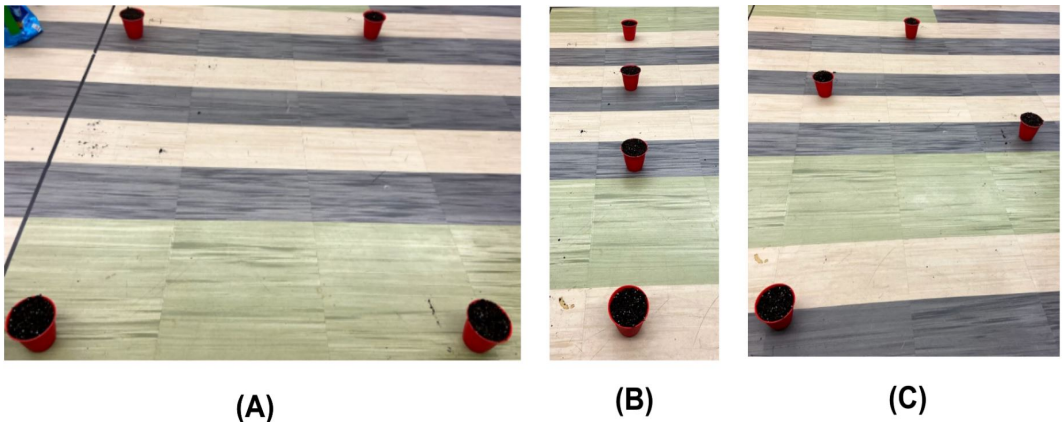

Figure 3.17: Soil Navigation and Sensing Setup (A): Square Soil Pot Configuration, (B) Straight Soil Pot Configuration (C) Random Soil Pot Configuration

3.4 Discussion

A mechanical design as well as phenotyping and navigation systems were proposed for MARIA and validated in a controlled setting. Navigation was tested using both indoor and outdoor global localization systems and was able to perform with a low root mean square error. Additionally a soil sensing manipulator was designed and implemented. Its ability to measure temperature and humidity was validated in a conditioned soil pot. Finally, the navigation system and soil sensing system were combined and allowed the rover to reach a specific global waypoint and perform a temperature and humidity sensing operation. With an actuated LiDAR, MARIA was also able to perform non-contact phenotyping with low percent error in plant height and volume estimation.

In future work there are many improvements that can be implemented. The drive system for MARIA is able to drive well in flat settings but is sensitive to bumps and uneven ground. As such the addition of a suspension system to the rover would reduce disturbances.

The manipulator onboard MARIA could be improved with better actuators that are able to handle larger loads. With higher torque the motors can handle harder soil. Additionally more degrees of freedom can be added to manipulators to handle more complex manipulator tasks that could be tailored to the specific needs of the crop of interest. The soil sampling end effector could also be further improved by adding the ability to eject soil samples into an internal soil storage container or store and collect a new soil sampling cartridge.

The tool changer at the end of the onboard manipulator could have additional end effectors designed. One end effector could be created such as weed spraying end effector. The tool changer could additionally have power contacts that can allow for power transfer. This could be used to connect to a charger and charge an onboard battery unit. A relay system could be used further to let these contacts deliver power to an end effector.

3.5 Conclusions and Limitations

In this paper a multipurpose agriculture robot design, named MARIA, is proposed using off-the-shelf components. An autonomous drive system is proposed using global localization systems for navigation and waypoint following. The phenotyping capability for MARIA was validated using an actuated lidar for measuring important phenotypic characteristics such as volume and height. A mobile three DoF actuator was designed for MARIA with a multipurpose end effector. The multipurpose end effector is able to be changed to various end effectors such as a drill or soil sampler. The mobile manipulator is additionally able to measure root zone temperature and moisture. This system has been validated in an indoor as well as a controlled outdoor setting. However there are multiple improvements needed to work robustly in the outdoor setting.

This work contributes to the field by presenting a design capable of both LiDAR phenotyping and soil sensing that could be easily replicated through use of off-shelf and 3D printed components. MARIA's design may help to reduce the barrier preventing the adoption of these robotics systems in the field, as most systems are not commercially available or require custom, difficult-to-manufacture components. Future work will be aimed at increasing the robustness and ease of use of this system in the field.

Chapter 4

Conclusion

This work aims to add to the development of agricultural robotics to alleviate the phenotyping bottleneck in which the high labor cost of manual phenotyping hinders the development of new, robust crops. Here, an autonomous mobile robot for navigation and phenotyping in an agricultural setting is proposed.

In the first section of this work, a simulation of a novel, customized mobile platform for autonomous phenotyping that can simultaneously phenotype and navigate through occluded crop rows is presented. A complete ROS configuration was implemented to represent an agriculture robot for HTP. A high fidelity simulated cotton crop environment was created as a testbed for phenotyping and navigation strategies. We propose the use of an actuated LiDAR configuration, which actively generates point cloud data simultaneously to be used for phenotyping as well as navigation. The efficacy of the nodding lidar configuration for phenotyping was tested against three common 2D LiDAR based phenotyping strategies and it was shown to be comparatively accurate as the current 2D LiDAR based strategy for determining volume and height of cotton plants. For navigation, a strategy was presented that uses a hybrid approach of LiDAR based control algorithm as well as GPS waypoint navigation. The proposed control algorithm uses the LiDAR point cloud generated by the actuated LiDAR configuration and ensures that the robot stays centered between crop rows. The proposed navigation strategy was able to successfully navigate between four cotton crop rows with .2% error.

In the next section, a multipurpose agriculture robot design, named MARIA, is proposed that utilizes the actuated LiDAR configuration tested previously in simulation for navigation and simulation. An autonomous drive system is proposed using global localization systems for navigation and waypoint following. The phenotyping capability of MARIA to measure plant height and volume was also tested. Additionally, a mobile three DoF actuator was designed for MARIA with a multipurpose end effector that is able to be changed to various effectors such as a drill or soil sampler. The mobile manipulator is additionally able to measure root zone temperature and moisture.

This work contributes to the field by presenting an open source design that could be easily replicated through use of off-shelf and 3D printed components. MARIA's design may help to reduce the barrier preventing the adoption of these robotics systems in the field, as most systems are not commercially available or require custom, difficult-to-manufacture components. The actuated LiDAR configuration

which allows for simultaneous navigation and phenotyping lowers the cost of development as two separate systems for navigation and phenotyping are not needed. This further lowers the barrier of entry into agricultural robotics and high-throughput phenotyping.

Bibliography

Åstrand, B., & Baerveldt, A.-J. (2002). An agricultural mobile robot with Vision-Based perception for mechanical weed control. *Auton. Robots*, *13*(1), 21–35.

Bakker, T., Asselt, K., Bontsema, J., Müller, J., & Straten, G. (2010). Systematic design of an autonomous platform for robotic weeding. *Journal of Terramechanics*, *47*(2), 63–73. https://doi.org/https://doi.org/10.1016/j.jterra.2009.06.002

Bascetta, L., Baur, M., & Gruosso, G. (2017). ROBI': A prototype mobile manipulator for agricultural applications. *Electronics*, *6*(2), 39.

Bietresato, M., Carabin, G., D'Auria, D., Gallo, R., Ristorto, G., Mazzetto, F., Vidoni, R., Gasparetto, A., & Scalera, L. (2016). A tracked mobile robotic lab for monitoring the plants volume and health, In *2016 12th ieee/asme international conference on mechatronic and embedded systems and applications (mesa)*.

Bitella, G., Rossi, R., Bochicchio, R., Perniola, M., & Amato, M. (2014). A novel low-cost open-hardware platform for monitoring soil water content and multiple soil-air-vegetation parameters. *Sensors*, *14*(10), 19639–19659.

Blackmore, B., Griepentrog, H. W., Nielsen, H., Nørremark, M., & Resting-Jeppesen, J. (2004). Development of a deterministic autonomous tractor.

Bogue, R. (2016). Robots poised to revolutionise agriculture. *Ind. Rob.*, *43*(5), 450–456.

Bonadies, S., & Gadsden, S. A. (2019). An overview of autonomous crop row navigation strategies for unmanned ground vehicles. *Engineering in Agriculture, Environment and Food*, *12*(1), 24–31. https://doi.org/https://doi.org/10.1016/j.eaef.2018.09.001

Bosse, M., Zlot, R., & Flick, P. (2012). Zebedee: Design of a spring-mounted 3-d range sensor with application to mobile mapping. *IEEE Transactions on Robotics*, *28*(5), 1104–1119. https://doi.org/10.1109/TRO.2012.2200990

Campbell, Z. C., Acosta-Gamboa, L. M., Nepal, N., & Lorence, A. (2018). Engineering plants for tomorrow: How high-throughput phenotyping is contributing to the development of better crops. *Phytochemistry reviews*, *17*(6), 1329–1343.

Fiorani, F., & Schurr, U. (2013). Future scenarios for plant phenotyping. *Annu Rev Plant Biol*, *64*, 267–91. https://doi.org/10.1146/annurev-arplant-050312-120137

Fountas, S., Mylonas, N., Malounas, I., Rodias, E., Hellmann Santos, C., & Pekkeriet, E. (2020). Agricultural robotics for field operations. *Sensors*, *20*(9).

French, A., Gore, M., & Thompson, A. (2016). *Cotton phenotyping with lidar from a track-mounted platform* (Vol. 9866). SPIE. https://doi.org/10.1117/12.2224423

Furbank, R. T., & Tester, M. (2011). Phenomics – technologies to relieve the phenotyping bottleneck. *Trends in Plant Science*, *16*(12), 635–644. https://doi.org/https://doi.org/10.1016/j.tplants.2011.09.005

Gonzalez-de-Santos, P., Ribeiro, A., Fernandez-Quintanilla, C., Lopez-Granados, F., Brandstoetter, M., Tomic, S., Pedrazzi, S., Peruzzi, A., Pajares, G., Kaplanis, G., Perez-Ruiz, M., Valero, C., del Cerro, J., Vieri, M., Rabatel, G., & Debilde, B. (2017). Fleets of robots for environmentally-safe pest control in agriculture. *Precis. Agric.*, *18*(4), 574–614.

Grimstad, L., & From, P. (2018). Software components of the thorvald ii modular robot. *Modeling, Identification and Control: A Norwegian Research Bulletin*, *39*, 157–165. https://doi.org/10.4173/mic.2018.3.2

Grimstad, L., & From, P. J. (2017). The thorvald II agricultural robotic system. *Robotics*, *6*(4), 24.

Habibie, N., Nugraha, A. M., Anshori, A. Z., Ma'sum, M. A., & Jatmiko, W. (n.d.). Fruit mapping mobile robot on simulated agricultural area in gazebo simulator using simultaneous localization and mapping (slam), In *2017 international symposium on micro-nanomechatronics and human science (mhs)*. https://doi.org/10.1109/MHS.2017.8305235

Harchowdhury, A., Kleeman, L., & Vachhani, L. (2018a). Coordinated nodding of a two-dimensional lidar for dense three-dimensional range measurements. *IEEE Robotics and Automation Letters*, *3*(4), 4108–4115. https://doi.org/10.1109/LRA.2018.2852781

Harchowdhury, A., Kleeman, L., & Vachhani, L. (2018b). Coordinated nodding of a Two-Dimensional lidar for dense Three-Dimensional range measurements. *IEEE Robotics and Automation Letters*, *3*(4), 4108–4115.

Hassan, M. U., Ullah, M., & Iqbal, J. (2016). Towards autonomy in agriculture: Design and prototyping of a robotic vehicle with seed selector, In *2016 2nd international conference on robotics and artificial intelligence (ICRAI)*.

He, Y., Yang, J., Zhu, B., & Zhu, Z. (2014). Low root zone temperature exacerbates the ion imbalance and photosynthesis inhibition and induces antioxidant responses in tomato plants under salinity. *Journal of Integrative Agriculture*, *13*, 89–99. https://doi.org/10.1016/S2095-3119(13)60586-9

Hector_gazebo_plugins - ROS wiki [Accessed: 2020-5-31]. (n.d.).

Higuti, V. A. H., Velasquez, A. E. B., Magalhaes, D. V., Becker, M., & Chowdhary, G. (2019). Under canopy light detection and ranging-based autonomous navigation. *Journal of Field Robotics*, *36*(3), 547–567. https://doi.org/10.1002/rob.21852

Jannink, J. L., Lorenz, A. J., & Iwata, H. (2010). Genomic selection in plant breeding: From theory to practice. *Brief Funct Genomics*, *9*(2), 166–77. https://doi.org/10.1093/bfgp/elq001

Jiang, Y., Li, C., & Paterson, A. H. (2016). High throughput phenotyping of cotton plant height using depth images under field conditions. *Computers and Electronics in Agriculture*, *130*, 57–68. https://doi.org/https://doi.org/10.1016/j.compag.2016.09.017

Jimenez-Berni, J. A., Deery, D. M., Rozas-Larraondo, P., Condon, A. G., Rebetzke, G. J., James, R. A., Bovill, W. D., Furbank, R. T., & Sirault, X. R. R. (2018). High throughput determination of plant height, ground cover, and above-ground biomass in wheat with lidar. *Frontiers in Plant Science*, *9*(237). https://doi.org/10.3389/fpls.2018.00237

Jimenez-Berni, J. A., Deery, D. M., Rozas-Larraondo, P., Condon, A. T. G., Rebetzke, G. J., James, R. A., Bovill, W. D., Furbank, R. T., & Sirault, X. R. R. (2018). High throughput determination of plant height, ground cover, and Above-Ground biomass in wheat with LiDAR. *Front. Plant Sci.*, *9*, 237.

Jin, S., Su, Y., Wu, F., Pang, S., Gao, S., Hu, T., Liu, J., & Guo, Q. (2019). Stem–leaf segmentation and phenotypic trait extraction of individual maize using terrestrial lidar data. *IEEE Transactions on Geoscience and Remote Sensing*, *57*(3), 1336–1346.

Kayacan, E., Zhang, Z., & Chowdhary, G. (2018). Embedded high precision control and corn stand counting algorithms for an Ultra-Compact 3D printed field robot, In *Robotics: Science and systems XIV*, Robotics: Science; Systems Foundation.

Kragh, M., Jørgensen, R. N., & Pedersen, H. (n.d.). Object detection and terrain classification in agricultural fields using 3d lidar data, Springer International Publishing.

Le, T. D., Ponnambalam, V. R., Gjevestad, J. G. O., & From, P. J. (n.d.). A low-cost and efficient autonomous row-following robot for food production in polytunnels. *Journal of Field Robotics*, *n/a*(n/a). https://doi.org/10.1002/rob.21878

Llop, J., Gil, E., Llorens, J., Miranda-Fuentes, A., & Gallart, M. (2016a). Testing the suitability of a terrestrial 2d lidar scanner for canopy characterization of greenhouse tomato crops. *Sensors*, *16*(9), 1435. https://www.mdpi.com/1424-8220/16/9/1435

Llop, J., Gil, E., Llorens, J., Miranda-Fuentes, A., & Gallart, M. (2016b). Testing the suitability of a terrestrial 2D LiDAR scanner for canopy characterization of greenhouse tomato crops. *Sensors*, *16*(9).

Łukowska, A., Tomaszuk, P., Dzierżek, K., & Magnuszewski, Ł. (2019). Soil sampling mobile platform for agriculture 4.0, In *2019 20th international carpathian control conference (ICCC)*.

Luo, X., Zhang, Z., Zhao, Z., Chen, B., Hu, L., & Wu, X. (2009). Design of dgps navigation control system for dongfanghong x-804 tractor. *Nongye Gongcheng Xuebao/Transactions of the Chinese Society of Agricultural Engineering*, *25*, 139–145. https://doi.org/10.3969/j.issn.1002-6819.2009.11.025

Malavazi, F. B. P., Guyonneau, R., Fasquel, J.-B., Lagrange, S., & Mercier, F. (2018a). LiDAR-only based navigation algorithm for an autonomous agricultural robot. *Comput. Electron. Agric.*, *154*, 71–79.

Malavazi, F. B. P., Guyonneau, R., Fasquel, J.-B., Lagrange, S., & Mercier, F. (2018b). Lidar-only based navigation algorithm for an autonomous agricultural robot. *Computers and Electronics in Agriculture*, *154*, 71–79. https://doi.org/https://doi.org/10.1016/j.compag.2018.08.034

MasayasuIwase. (n.d.). Scanning rangefinder distance data Output/UTM-30LX product details | HOKUYO AUTOMATIC CO., LTD.

Mousazadeh, H. (2013). A technical review on navigation systems of agricultural autonomous off-road vehicles. *Journal of Terramechanics*, *50*(3), 211–232. https://doi.org/https://doi.org/10.1016/j.jterra.2013.03.004

Mueller-Sim, T., Jenkins, M., Abel, J., & Kantor, G. (n.d.). The robotanist: A ground-based agricultural robot for high-throughput crop phenotyping, In *2017 ieee international conference on robotics and automation (icra)*. https://doi.org/10.1109/ICRA.2017.7989418

Mueller-Sim, T., Jenkins, M., Abel, J., & Kantor, G. (2017). The robotanist: A ground-based agricultural robot for high-throughput crop phenotyping. https://doi.org/10.1109/ICRA.2017.7989418

Nagasaka, Y., Saito, H., Tamaki, K., Seki, M., Kobayashi, K., & Taniwaki, K. (2009). An autonomous rice transplanter guided by global positioning system and inertial measurement unit. *Journal of Field Robotics*, *26*(6-7), https://onlinelibrary.wiley.com/doi/pdf/10.1002/rob.20294, 537–548. https://doi.org/10.1002/rob.20294

Nakamoto, T. (1995). Gravitropic reaction of primary seminal roots of zea mays l. influenced by temperature and soil water potential. *J. Plant Res.*, *108*(1089), 71–75.

Normey-Rico, J. E., Alcalá, I., Gómez-Ortega, J., & Camacho, E. F. (2001). Mobile robot path tracking using a robust pid controller [PID Control]. *Control Engineering Practice*, *9*(11), 1209–1214. https://doi.org/https://doi.org/10.1016/S0967-0661(01)00066-1

Ollero, A., & Heredia, G. (1995). Stability analysis of mobile robot path tracking, In *Proceedings 1995 ieee/rsj international conference on intelligent robots and systems. human robot interaction and cooperative robots*.

Pabuayon, I. L. B., Sun, Y., Guo, W., & Ritchie, G. L. (2019a). High-throughput phenotyping in cotton: A review. *Journal of Cotton Research*, *2*(1), 18. https://doi.org/10.1186/s42397-019-0035-0

Pabuayon, I. L. B., Sun, Y., Guo, W., & Ritchie, G. L. (2019b). High-throughput phenotyping in cotton: A review. *Journal of Cotton Research*, *2*(1), 18.

Passioura, J. B. (2012). Phenotyping for drought tolerance in grain crops: When is it useful to breeders? *Funct. Plant Biol.*, *39*(11), 851–859.

Pedersen, S. M., Fountas, S., Have, H., & Blackmore, B. S. (2006). Agricultural robots—system analysis and economic feasibility. *Precision Agriculture*, *7*(4), 295–308. https://doi.org/10.1007/s11119-006-9014-9

Pobkrut, T., & Kerdcharoen, T. (2014). Soil sensing survey robots based on electronic nose, In *2014 14th international conference on control, automation and systems (ICCAS 2014)*.

Rahul, K., Raheman, H., & Paradkar, V. (2019). Design and development of a 5R 2DOF parallel robot arm for handling paper pot seedlings in a vegetable transplanter. *Comput. Electron. Agric.*, *166*, 105014.

Reina, G., Milella, A., Rouveure, R., Nielsen, M., Worst, R., & Blas, M. R. (2016). Ambient awareness for agricultural robotic vehicles [Special Issue: Advances in Robotic Agriculture for Crops]. *Biosystems Engineering*, *146*, 114–132. https://doi.org/https://doi.org/10.1016/j.biosystemseng.2015.12.010

Reiser, D., Vázquez-Arellano, M., Paraforos, D. S., Garrido-Izard, M., & Griepentrog, H. W. (2018). Iterative individual plant clustering in maize with assembled 2d lidar data. *Computers in Industry*, *99*, 42–52. https://doi.org/https://doi.org/10.1016/j.compind.2018.03.023

Robot_localization. (n.d.).

Rovira-Más, F., Chatterjee, I., & Sáiz-Rubio, V. (2015). The role of gnss in the navigation strategies of cost-effective agricultural robots [Precision Agriculture]. *Computers and Electronics in Agriculture*, *112*, 172–183. https://doi.org/https://doi.org/10.1016/j.compag.2014.12.017

Ruckelshausen, A., Biber, P., Dorna, M., Gremmes, H., Klose, R., Linz, A., Rahe, F., Resch, R., Thiel, M., Trautz, D., Et al. (2009). BoniRob–an autonomous field robot platform for individual plant phenotyping. *Precis. Agric.*, *9*(841), 1.

Samuel, M., Hussein, M., & Mohamad, M. B. (2016). A review of some pure-pursuit based path tracking techniques for control of autonomous vehicle. *International Journal of Computer Applications*, *135*(1), 35–38.

Scholz, C., Möller, K., Ruckelshausen, A., Hinck, S., & Göttinger, M. (2014). Automatic soil penetrometer measurements and gis-based documentation with the autonomous field robot platform bonirob.

Shafiekhani, A., Kadam, S., Fritschi, F. B., & DeSouza, G. N. (2017). Vinobot and vinoculer: Two robotic platforms for High-Throughput field phenotyping. *Sensors*, *17*(1).

Shamshiri, R., Hameed, I., Karkee, M., & Weltzien, C. (2018). Robotic harvesting of fruiting vegetables, a simulation approach in v-rep, ros and matlab. https://doi.org/10.5772/intechopen.73861

Shamshiri, R., Hameed, I., Pitonakova, L., Weltzien, C., Balasundram, S., Yule, I., Grift, T., & Chowdhary, G. (2018). Simulation software and virtual environments for acceleration of agricultural robotics: Features highlights and performance comparison. *International Journal of Agricultural and Biological Engineering*, *11*, 12–20. https://doi.org/10.25165/j.ijabe.20181103.4032

Sharifi, M., Young, M. S., Chen, X., Clucas, D., & Pretty, C. (2016). Mechatronic design and development of a non-holonomic omnidirectional mobile robot for automation of primary production. *Cogent Engineering*, *3*(1). https://doi.org/10.1080/23311916.2016.1250431

Stager, A., Tanner, H. G., & Sparks, E. E. (2019). Design and construction of unmanned ground vehicles for Sub-Canopy plant phenotyping, arXiv 1903.10608.

Sun, S., Li, C., & Paterson, A. H. (2017). In-field high-throughput phenotyping of cotton plant height using lidar. *Remote Sensing*, *9*(4), 377. https://www.mdpi.com/2072-4292/9/4/377

Sun, S., Li, C., Paterson, A. H., Jiang, Y., Xu, R., Robertson, J. S., Snider, J. L., & Chee, P. W. (2018a). In-field high throughput phenotyping and cotton plant growth analysis using lidar. *Frontiers in Plant Science*, *9*(16). https://doi.org/10.3389/fpls.2018.00016

Sun, S., Li, C., Paterson, A. H., Jiang, Y., Xu, R., Robertson, J. S., Snider, J. L., & Chee, P. W. (2018b). In-field high throughput phenotyping and cotton plant growth analysis using LiDAR. *Front. Plant Sci.*, *9*, 16.

Van Der Weide, R. Y., Bleeker, P. O., Achten, V. T. J. M., Lotz, L. A. P., Fogelberg, F., & Melander, B. (2008). Innovation in mechanical weed control in crop rows. *Weed Res.*, *48*(3), 215–224.

Velasquez, A., Higuti, V., Borrero GUerrero, H., Valverde Gasparino, M., Magalhães, D., Aroca, R., & Becker, M. (2019). Reactive navigation system based on h control system and lidar readings on corn crops. *Precision Agriculture*. https://doi.org/10.1007/s11119-019-09672-8

Vidoni, R., Gallo, R., Ristorto, G., Carabin, G., Mazzetto, F., Scalera, L., & Gasparetto, A. (2017). Byelab: An agricultural mobile robot prototype for proximal sensing and precision farming. https://doi.org/10.1115/IMECE2017-71216

Wang, H., Lin, Y., Wang, Z., Yao, Y., Zhang, Y., & Wu, L. (2017a). Validation of a low-cost 2d laser scanner in development of a more-affordable mobile terrestrial proximal sensing system for 3d plant structure phenotyping in indoor environment. *Computers and Electronics in Agriculture*, *140*, 180–189. https://doi.org/https://doi.org/10.1016/j.compag.2017.06.002

Wang, H., Lin, Y., Wang, Z., Yao, Y., Zhang, Y., & Wu, L. (2017b). Validation of a low-cost 2D laser scanner in development of a more-affordable mobile terrestrial proximal sensing system for 3D plant structure phenotyping in indoor environment. *Comput. Electron. Agric.*, *140*, 180–189.

Watt, M., Silk, W. K., & Passioura, J. B. (2006). Rates of root and organism growth, soil conditions, and temporal and spatial development of the rhizosphere. *Ann. Bot.*, *97*(5), 839–855.

Weiss, U., & Biber, P. (2011). Plant detection and mapping for agricultural robots using a 3d lidar sensor. *Robotics and Autonomous Systems*, *59*(5), 265–273. https://doi.org/https://doi.org/10.1016/j.robot.2011.02.011

White, J. W., Andrade-Sanchez, P., Gore, M. A., Bronson, K. F., Coffelt, T. A., Conley, M. M., Feldmann, K. A., French, A. N., Heun, J. T., Hunsaker, D. J., Jenks, M. A., Kimball, B. A., Roth, R. L., Strand, R. J., Thorp, K. R., Wall, G. W., & Wang, G. (2012a). Field-based phenomics for plant genetics research. *Field Crops Research*, *133*, 101–112. https://doi.org/https://doi.org/10.1016/j.fcr.2012.04.003

White, J. W., Andrade-Sanchez, P., Gore, M. A., Bronson, K. F., Coffelt, T. A., Conley, M. M., Feldmann, K. A., French, A. N., Heun, J. T., Hunsaker, D. J., Jenks, M. A., Kimball, B. A., Roth, R. L., Strand, R. J., Thorp, K. R., Wall, G. W., & Wang, G. (2012b). Field-based phenomics for plant genetics research. *Field Crops Res.*, *133*, 101–112.

YANG, L., & NOGUCHI, N. (2014). Development of a wheel-type robot tractor and its utilization [19th IFAC World Congress]. *IFAC Proceedings Volumes*, *47*(3), 11571–11576. https://doi.org/https://doi.org/10.3182/20140824-6-ZA-1003.00952

Zhang, L., & Grift, T. E. (2012). A lidar-based crop height measurement system for miscanthus giganteus. *Computers and Electronics in Agriculture*, *85*, 70–76. https://doi.org/https://doi.org/10.1016/j.compag.2012.04.001

Zotz, G., Hietz, P., & Schmidt, G. (2001). Small plants, large plants: The importance of plant size for the physiological ecology of vascular epiphytes. *Journal of Experimental Botany*, *52*(363), 2051–2056. https://doi.org/10.1093/jexbot/52.363.2051